Seismic Tomography of Concrete Structures

Phase II: Hardware and Software Developments
Phase III: Field Tests at Seminoe Dam

Dam Safety Office

Report No. DSO-02-03
Department of the Interior
Bureau of Reclamation
September 2002

REPORT DOCUMENTATION PAGE

Form Approved
OMB No. 0704-0188

1. AGENCY USE ONLY *(Leave Blank)*	2. REPORT DATE	3. REPORT TYPE AND DATES COVERED
	September 2002	

4. TITLE AND SUBTITLE
Seismic Tomography of Concrete Structures
Phase II: Hardware and Software Developments
Phase III: Field Tests at Seminoe Dam

5. FUNDING NUMBERS
.

6. AUTHOR(S)
Lisa Block

7. PERFORMING ORGANIZATION NAME(S) AND ADDRESS(ES)
Bureau of Reclamation
Denver Federal Center
P.O. Box 25007
Denver, CO 80225-0007

8. PERFORMING ORGANIZATION REPORT NUMBER
DSO-02-02

9. SPONSORING/MONITORING AGENCY NAME(S) AND ADDRESS(ES)
Same

10. SPONSORING/MONITORING AGENCY REPORT NUMBER
DIBR

11. SUPPLEMENTARY NOTES

12a. DISTRIBUTION/AVAILABILITY STATEMENT
Available from the National Technical Information Service, Operations Division, 5285 Port Royal Road, Springfield, Virginia 22161

12b. DISTRIBUTION CODE

13. ABSTRACT ***(Maximum 200 words)***

Between 1997 and 2001, the Seismotectonics and Geophysics Group at the Bureau of Reclamation conducted a research project on the application of the seismic tomography method to investigation of large concrete structures. The hardware and software needed to efficiently acquire high-quality seismic tomography data on large concrete structures were developed. This hardware and software, as well as the effectiveness of the seismic tomography method as applied to concrete structures, was evaluated by acquiring and processing seismic tomography data from a concrete arch dam undergoing alkali-aggregate reaction. A total of approximately 13,700 seismic waveforms were acquired across three upstream-downstream cross sections during 9 days of data acquisition. Seismic ray paths ranging from horizontal to approximately 70 degrees from horizontal were obtained through most of each cross section, with excellent signal-to-noise ratio on most seismic traces. The P-wave velocity tomograms computed from these data show velocities ranging from 16,000 ft/s to less than 7,000 ft/s. The areas with the lowest P-wave velocities are interpreted as regions with the most severely deteriorated concrete. The pattern of P-wave velocity variations is consistent with information obtained from core analyses, fracture mapping, and deformation studies, and provides valuable additional information about the spatial distribution of concrete deterioration.

14. SUBJECT TERMS
seismic tomography
nondestructive testing
alkali-aggregate reaction
alkali-silica reaction
travel-time tomography
velocity tomogram
concrete deterioration

15. NUMBER OF PAGES
68

16. PRICE CODE

17. SECURITY CLASSIFICATION OF REPORT	18. SECURITY CLASSIFICATION OF THIS PAGE	19. SECURITY CLASSIFICATION OF ABSTRACT	20. LIMITATION OF ABSTRACT
UC	UC	UC	UC

Prepared by

Lisa Block
Geophysicist

9/18/2002
Date

Peer review by

Jerry Wright
Manager, Geophysics
and Seismotectonics Group

9/18/02
Date

TABLE OF CONTENTS

LIST OF FIGURES

LIST OF TABLES

1.0 INTRODUCTION

Between 1997 and 2001, the Geophysics and Seismotectonics Group conducted a research project on the application of the seismic tomography method to investigate large concrete structures. This project has been largely funded by the Dam Safety Office, with supplemental funding of equipment purchases from the Technical Service Center. The goal of this research project is to develop Reclamation's capabilities for efficiently acquiring high-quality seismic tomography data on concrete structures for the purpose of imaging variations in concrete quality within the structure. The hardware and software developed during this project and the effectiveness of the seismic tomography method as applied to concrete structures has been evaluated by acquiring and processing seismic tomography data from Seminoe Dam, a concrete arch dam located in south-central Wyoming.

The project was divided into several major phases. Phase I, which consisted of gathering background information from other researchers and performing field and laboratory tests to determine which types of sources, receivers, and coupling methods are likely to produce the highest quality seismic data on concrete structures, was completed in fiscal year (FY) 1997. A report covering this phase was finalized in September 1998 (Block, 1998). Phase II consisted of developing hardware and software necessary for performing a full-scale field tomography survey. These steps included purchasing and constructing equipment, modifying data processing software, and developing survey design software. These steps were performed in FY97 and FY98 and are described in section 2.0 of this report. The seismic tomography equipment constructed for use on concrete structures is described in section 2.1, and the computer programs developed for data processing and survey design are described in section 2.2. Phase III consisted of data acquisition at Seminoe Dam and the processing of arrival times to construct P-wave velocity images. Initial data acquisition at Seminoe Dam along one tomography cross section was performed in April and September 1999. Data were acquired along 2 additional cross sections in August 2000. Preliminary results from these surveys were transmitted to the Dam Safety Office in 1999 and 2000 (Block, 1999; Block, 2000). The data acquisition and results are described more fully in section 3.0 of this report.

2.0 PHASE II - HARDWARE AND SOFTWARE DEVELOPMENTS

2.1 Field Equipment

Acquiring high-frequency seismic data with good signal-to-noise ratio and a high degree of repeatability on a concrete dam requires specialized equipment. The presence of a power plant and high-power transmission lines must also be considered. Cable shielding, line drivers, and amplifiers reduce the effects of the electromagnetic interference from these sources of power. Based on the results of equipment tests performed during Phase I of this research project, components were purchased and the following equipment was then assembled for acquiring seismic tomography data on concrete dams:

1. Two power-actuated fastening tools (nail guns), slightly modified to be used as repeatable, high-frequency seismic sources on concrete surfaces.

2. Three instrumented 2-lb sledge hammers for use as seismic sources.

3. A 16-receiver hydrophone string for recording seismic energy in the reservoir immediately upstream from a dam. The hydrophone string may also be used in boreholes.

4. Sixteen high-frequency accelerometers, mounted in rugged plastic cases with short pig-tail cables and connectors attached. These are stud-mounted on concrete surfaces for recording data.

5. A box containing amplifiers and power supplies for the accelerometers.

6. A 20-channel, high-speed data acquisition system. This system can handle higher frequencies and larger signal amplitudes than traditional geophysical industry seismographs.

7. Miscellaneous cables and connectors for use with all of the equipment described above.

This equipment is described in more detail below. Included in the descriptions below are comments regarding the performance of the equipment during the field tests conducted at Seminoe Dam.

2.1.1 Nail Gun Seismic Source

One seismic source selected for use in seismic tomography surveys is a power-actuated fastening tool, commonly called a nail gun. It is designed to drive nails and other fasteners into hard surfaces. We used the Remington model 495 fastening tool, purchased at a local hardware store. The piston in this tool is driven with 27 mm explosive cartridges. The cartridges come on plastic strips that are inserted into the bottom of the tool handle (figure 2-1a). Each strip contains 10 cartridges.

To use this tool as a seismic source, we welded a steel plate onto the end of the barrel of the nail gun. The plate has a hole in its center. This hole is the same size as the outer diameter of the

(a)

(b)

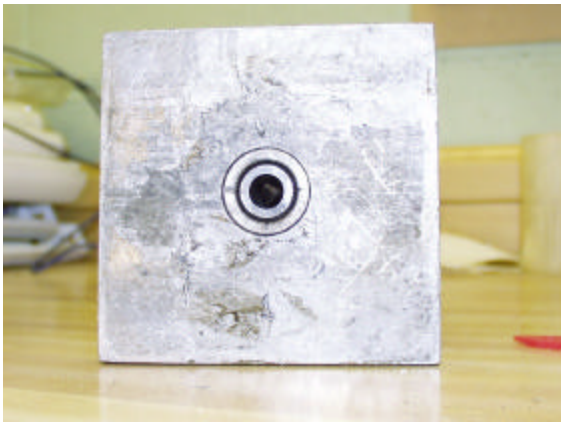

(c)

(d)

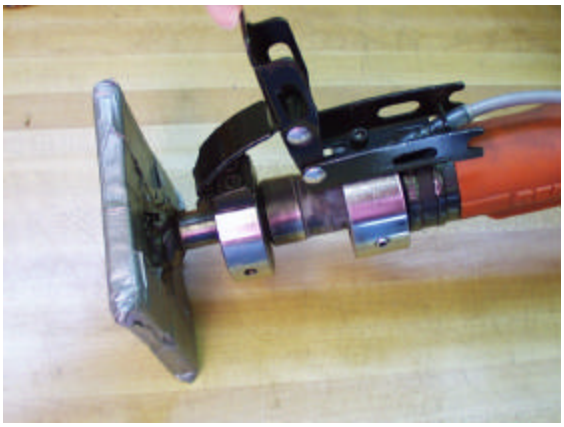

(e)

FIGURE 2-1: Power-actuated fastening tool (nail gun) used as a seismic source. (a) Tool with load strips (b) Front view of plate welded onto end of tool barrel (c) Disposable plate placed between tool and concrete surface (d) Clamping mechanism (e) Pulley system on nail guns.

barrel of the nail gun, so that the plate fits around the barrel and is flush with the barrel end (figure 2-1b). When the nail gun is used as a seismic source on a concrete surface, a disposable strike plate is placed between the welded plate and the concrete surface (figure 2-1c). The strike plate is made from wrought iron and is 1/4-inch thick. The piston of the nail gun strikes this iron plate. After 4 or 5 shots, the disposable strike plate is too warped to be used further and is replaced with a fresh one.

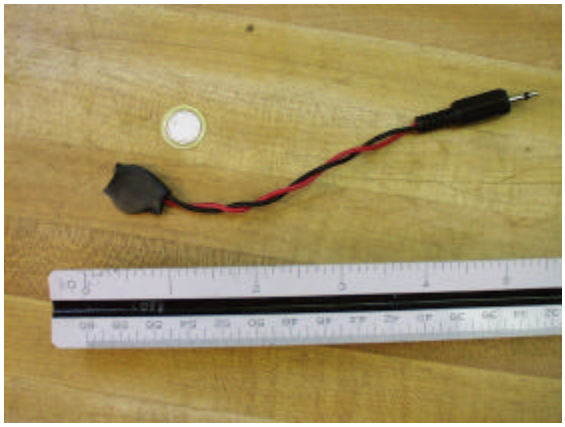

FIGURE 2-2: Piezoelectric transducer trigger. A transducer element is shown alone (white disc), and below is a transducer that has been wired for use as a trigger. The major increments on the upper side of the ruler are inches.

As a safety mechanism, the nail gun will not fire until the barrel is collapsed by pushing the end of the barrel against a hard surface. Because the climbers cannot apply enough force while hanging on ropes to collapse the barrel, we designed a clamping mechanism to collapse the barrel before firing (figure 2-1d). This clamping mechanism is simple, reliable, and easy to use. However, because this modification essentially bypasses the built-in safety mechanism for the tool, the Reclamation Safety Officer considered this modification to be unsafe and would not allow it to be used during the field tests. As an alternative, the climbers designed a pulley system for the tool to increase their leverage when collapsing the gun barrel (figure 2-1e). This method was more difficult to use than the clamping mechanism and seemed to produce less repeatable source impacts.

Two types of triggering mechanisms were tested for use with the nail gun. (The trigger sends a signal to the recording system to indicate the exact time of the source impact.) Initially, flat round piezoelectric transducers were tested. The transducers were wired with short cables and connectors (figure 2-2) and attached to the concrete surface using silicon sealant as an adhesive. The plan was to attach a transducer at each source location on the concrete dam and to move the trigger cable from one transducer to the next during data acquisition. The anticipated advantages of using this type of triggering device were: the piezoelectric transducers do not require power, attaching the trigger to the stationary concrete surface that is being impacted should give a cleaner trigger signal than attaching the trigger to the moving seismic source, and the trigger cable will not interfere with firing of the nail gun since it is not attached to the gun. While lab tests looked hopeful, field testing at Seminoe Dam clearly indicated that this type of trigger is inadequate. The trigger connectors repeatedly shorted out and some transducers failed. More importantly, the trigger signals did not give consistent, reliable indications of source impact. Typical signals from these triggers are shown in figure 2-3. Acoustic energy from the explosion of the charge and acceleration of the piston before impact interferes with the onset of the signal from the piston hitting the metal plate.

The second type of triggering mechanism designed for use with the nail gun source gave very good results during field testing. This mechanism consists of an electrical contact closure signal. A diagram of the contact closure circuit is shown in figure 2-4. A wire from one post of a 6-V battery is connected to the disposable metal strike plate, and a wire from the other battery post is connected to a metal section of the nail gun that has electrical contact with the piston. Two additional wires are attached to the same locations to record the signal. The metal plate welded on the end of the nail gun barrel is covered with duct tape to electrically isolate the nail gun from the strike plate.

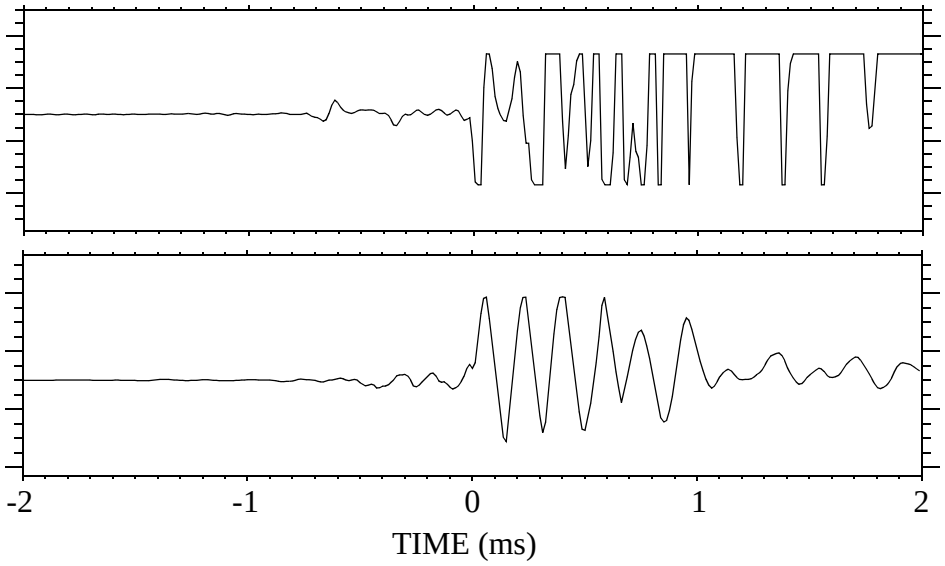

FIGURE 2-3: Waveforms from piezoelectric transducer triggers for the nail gun seismic source.

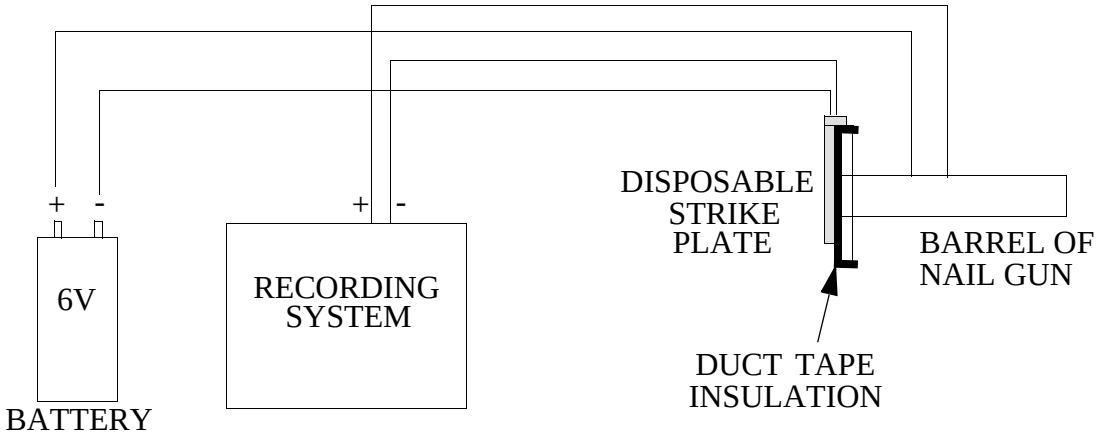

FIGURE 2-4: Diagram of the electrical contact closure trigger circuit for the nail gun seismic source.

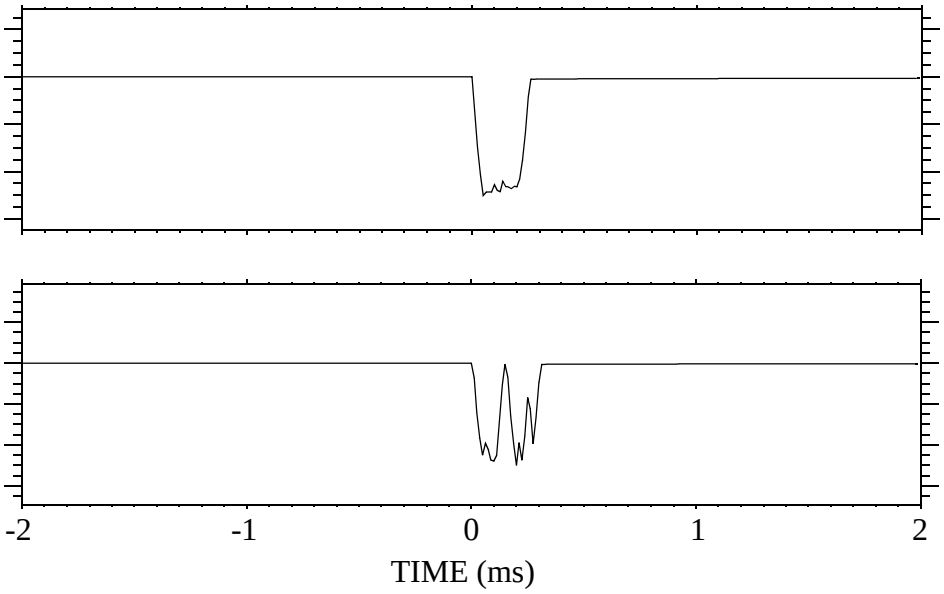

FIGURE 2-5: Waveforms from the electrical contact closure trigger for the nail gun seismic source.

When the piston contacts the strike plate, the measured voltage drops from 6 V to 0 V. Examples of the signal from this trigger are shown in figure 2-5. This trigger mechanism proved reliable and consistent in field testing, assuming that the climbers took care to prevent electrical contact between the plate and nail gun immediately before firing.

The primary advantage of this seismic source is the high-frequency energy it generates. Seismic signals acquired from the nail gun source are consistently higher in frequency than those acquired with the sledge hammer source (described below) (figure 2-6). (Signal-to-noise levels of data acquired with the two sources are comparable.) The spatial resolution of the tomographic images computed from the seismic tomography data is highly dependent on the frequency content of the waveforms. The higher the frequency content, the better the spatial resolution (i.e., the smaller the features that can be reliably imaged). Because of the higher frequencies generated with the nail gun source, data recorded with this source are considered to be of higher quality than those recorded with a sledge hammer source.

A significant disadvantage of this source encountered during field testing at Seminoe Dam is that mechanical problems greatly slowed data acquisition. As the nail gun was repeatedly fired, the gun became hot and the firing mechanism locked. The reason for the problem was not identified. It is possible that a U-bolt clamped onto the back end of the gun for attachment of a safety line may have contributed to this problem. When this bolt was originally clamped onto the tool, the resulting compression of the housing prevented the nail gun from firing. The bolt had to be rotated 90 degrees for the gun to fire. Perhaps, as the gun became heated and expanded slightly, the compression caused by the clamps began to interfere with the firing mechanism. Time constraints in the field prevented further testing of the nail gun source, and this issue remains unresolved.

2.1.2 Sledge Hammer Seismic Source

A 2-lb sledge hammer is used as another seismic source. A shock (high-impact) accelerometer stud-mounted onto the back of the hammer serves as the triggering mechanism (figure 2-7a; accelerometer specifications are included in appendix A). To protect the accelerometer and the small wires attached to it from damage, a 1/4-inch-thick rubber cylinder is clamped over the back of the hammer (figure 2-7b). This rubber cylinder is actually a pipe adaptor (1 1/2 to 1 1/4 inch) purchased at a local hardware store. A piece of duct tape is used to close off the end of the cylinder. The small wires attached to the accelerometer are spliced onto thicker wires within a jacketed cable (figure 2-7a), which is clamped beneath the rubber cylinder for strain relief (figure 2-7b). This cable is about 2 feet long, with a connector that attaches to the end of the trigger line. The single pair of wires within this cable carries both the power for the accelerometer (from a power supply at the other end of the trigger line) and the output accelerometer signal. Examples of signals obtained with the accelerometer trigger on the sledge hammer source are presented in figure 2-8.

An accelerometer was chosen for the triggering mechanism rather than an electrical contact closure signal for several reasons. Using the accelerometer trigger, the hammer can be hit directly on the concrete surface rather than on a metal plate. Striking the concrete surface rather than a metal plate is simpler (there are fewer pieces of equipment for the climbers to use) and is likely to give a cleaner, more impulsive signal (a metal plate can bounce, causing multiple impacts). Also, the source signature is recorded by the accelerometer. The source signature may be useful for performing tomography using amplitude or frequency information.

When using the accelerometer trigger, it is necessary to correct for the slight time delay between

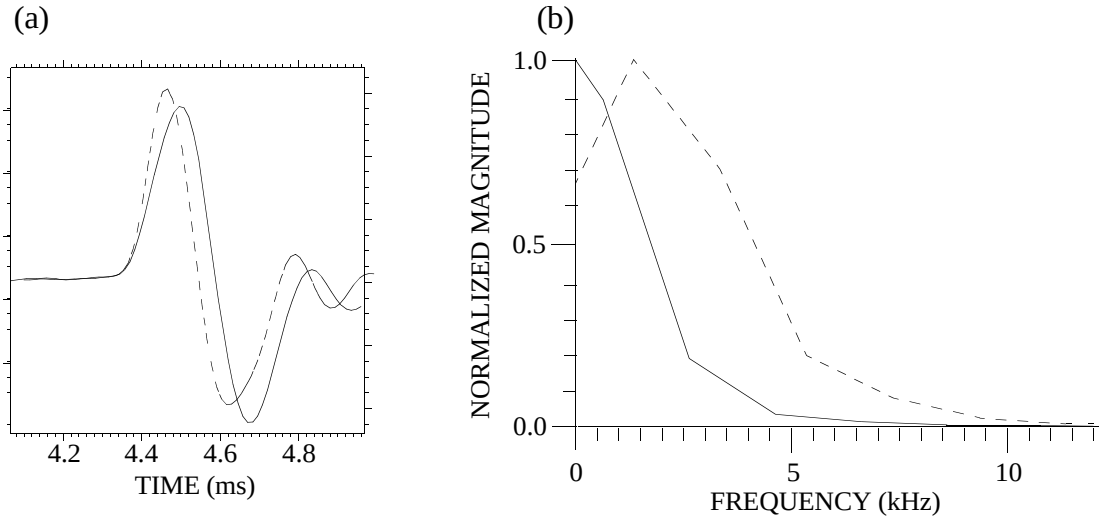

FIGURE 2-6: Comparison of signals obtained with the nail gun (dashed line) and sledge hammer (solid line) seismic sources. These signals were acquired for the same ray path (sources and receivers at the same locations). (a) Time-domain data (b) Frequency spectra.

(a) (b)

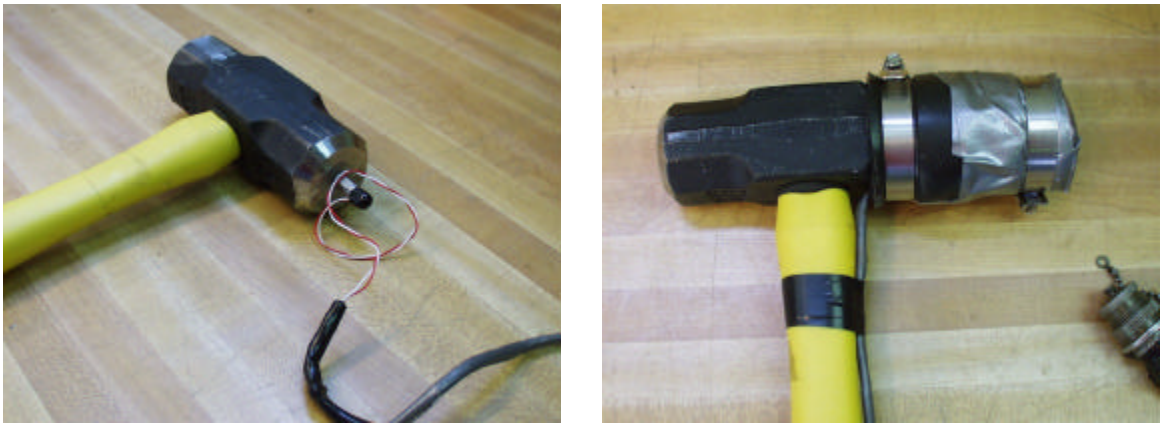

FIGURE 2-7: Sledge hammer seismic source. (a) Accelerometer trigger is stud-mounted on the back of the hammer head. (b) The accelerometer and wires are protected with a thick rubber cover.

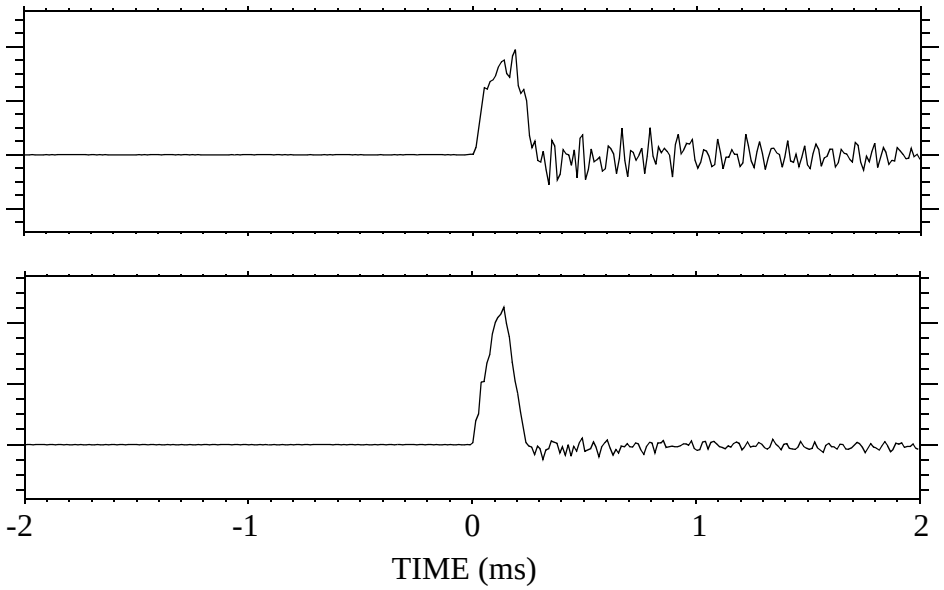

FIGURE 2-8: Waveforms from the accelerometer trigger for the sledge hammer seismic source.

source impact and output of the signal from the accelerometer. Although this delay is small, it can affect the computed tomograms because it is a consistent error. To measure this delay, 80 tests were performed using four different accelerometers. Signals from an electrical contact closure signal

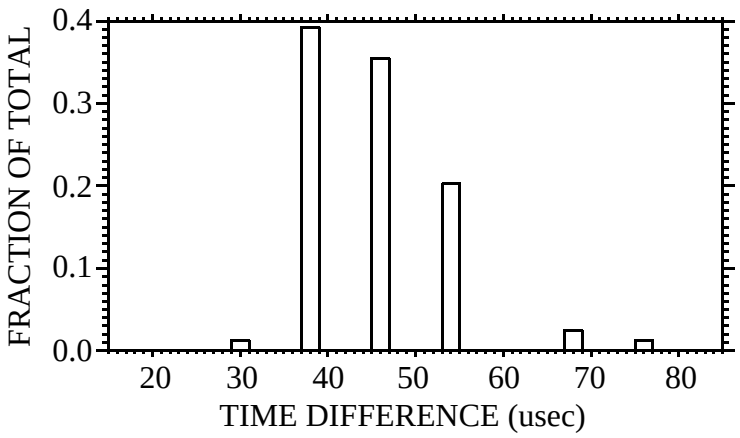

FIGURE 2-9: Normalized histogram of time differences measured in the laboratory between the response from an accelerometer mounted on a sledge hammer and an electrical contact closure signal. The data are from 80 tests performed with 4 different accelerometers.

between a sledge hammer and a metal strike plate and corresponding signals from an accelerometer mounted on the hammer were recorded simultaneously. The differences between the times of the contact closure and the first-break times on the accelerometer signal were measured. A histogram of the measured time differences is presented in figure 2-9. The discretization of the histogram is caused by the 7-μsec sampling interval of the recording system used. The median measured time difference is 45 μsec. Differences in delay times between different accelerometers were not significant. An inversion of field data acquired with the nail gun source using an electrical contact closure trigger and the sledge hammer source with the accelerometer trigger yields a computed time difference of 42 μsec for the two triggers, consistent with the value measured in the lab tests.

The accelerometer triggers performed well in the field. The trigger signals are generally consistent in appearance and have sharp first breaks. A few lower-frequency, more emergent trigger signals were recorded. These poorer quality trigger signals were associated with hammer hits on very soft concrete. Eventually, the accelerometers wear out, but they were found to perform well for thousands of impacts. The rubber cylinders stayed in place and adequately protected the accelerometers and wires.

2.1.3 Hydrophone String

A 16-channel hydrophone string was built for recording seismic data in the reservoir immediately upstream from a dam. Each hydrophone consists of a cylindrical piezoelectric transducer and an attached custom-designed amplifier board (figure 2-10a). Specifications for the hydrophone transducers and amplifiers are included in appendix A. The transducers have a flat frequency response to within 1.5 dB from 1 Hz to 15 kHz. (The response is within 2.5 dB to 25 kHz.) At these frequencies, they have an omnidirectional response. The amplifiers have a fixed gain of 32 dB and differential output. Each amplifier board was potted in epoxy to protect it from damage. Power for the amplifiers may be supplied by either the custom-designed recording system described below (section 2.1.6), or by two 12-volt batteries.

The 16 hydrophones are spaced 2 feet apart along a multi-conductor cable. The hydrophones

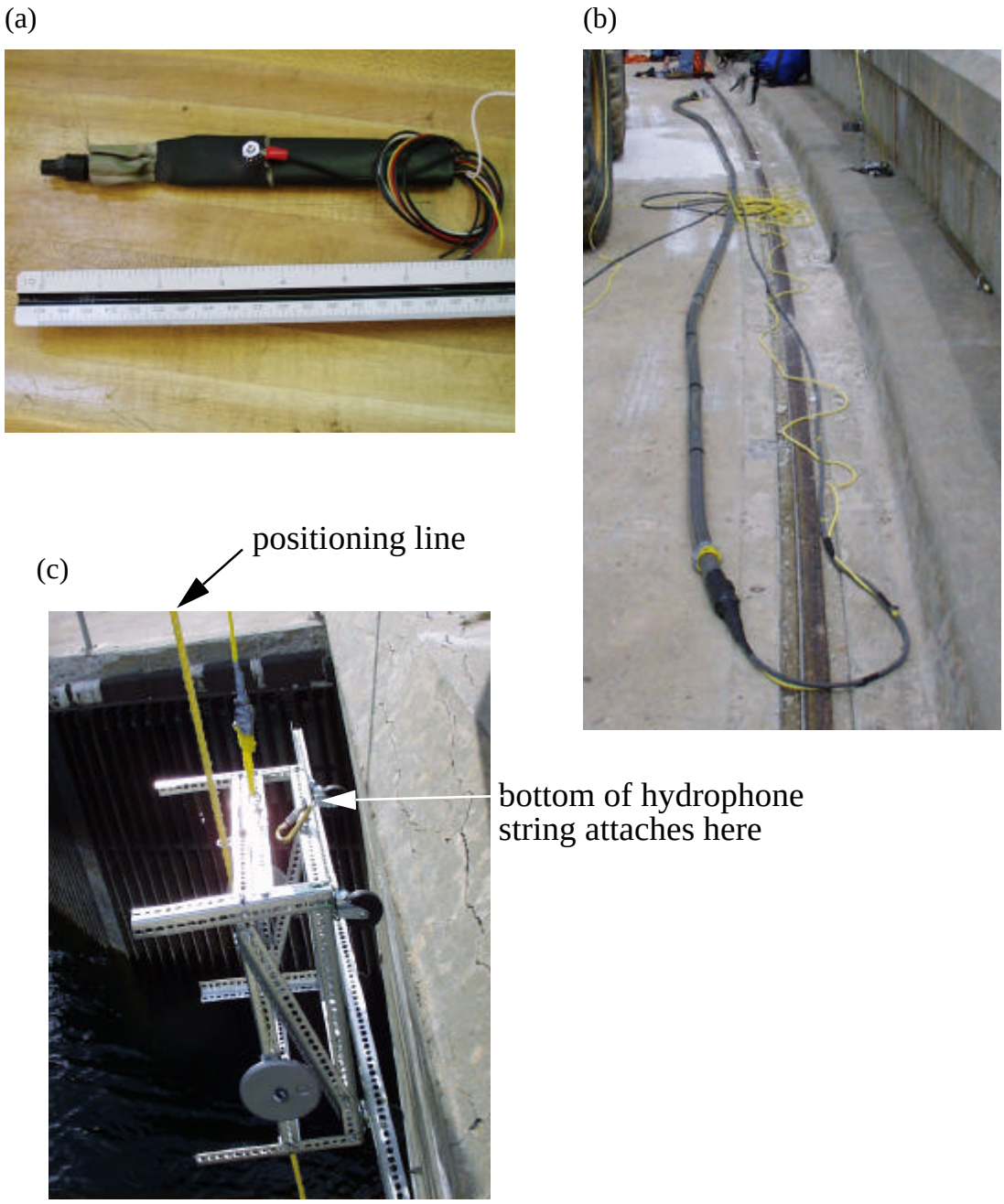

FIGURE 2-10: Hydrophone string and positioning line. (a) Cylindrical hydrophone cartridge attached to potted amplifier board. The major divisions on the upper side of the ruler are inches. (b) Hydrophone string attached to jumper cable. (c) Hydrophone positioning line (attached to a weight on the bottom of the reservoir) and cart.

and cable are enclosed in 2-inch outside diameter (O.D.) flexible plastic tubing (figure 2-10b). The tubing is filled with transmission oil to provide electrically non-conductive seismic coupling to the water. The top of the hydrophone string has a multi-pin underwater connector that attaches to a cable containing 18 twisted pairs of conductors. Sixteen of the pairs are used for transmitting the

hydrophone output signals to the recording system. The other two pairs are used for power and grounding.

The hydrophone string performed extremely well in field testing. There have been no problems with either the hydrophone cartridges themselves or the amplifiers. In addition, the hydrophone tubing, cables, and underwater connectors have performed well, with no leaks occurring.

The biggest problem with use of the hydrophone string in the reservoir upstream from a dam is keeping the string in a known position. Initially, a small weight (about 7 or 8 lbs) was attached to the bottom of the string to help it remain in a vertical position. This weight did not adequately prevent lateral drift of the hydrophone string. A heavily-weighted positioning line was later used. The weight (approximately 1,000 lbs) was lowered to the bottom of the reservoir. The bottom of the hydrophone string was attached to a cart that was run up and down the positioning line (figure 2-10c). This method yielded better results, but required significant field support in terms of heavy equipment required to move the weight. Also, borehole deviation surveys were run along the positioning line to determine the geometry of the positioning line (since the weight may have moved laterally after hitting the bottom of the reservoir.) These surveys were difficult to run accurately along a single line (small errors in the measured inclinations accumulate with depth), and the magnetometer within the deviation tool may have been affected by the presence of metal in the intake tower and trash rack. It may be better to keep the weight off the reservoir floor and simply assume that it is hanging vertically. It may also be better to attach the hydrophone string to the weight line (or between 2 weight lines) at multiple points. More options for positioning the hydrophone string should be investigated in the future. The methods used will depend on the geometry of the upstream dam face, the strength of the currents in the reservoir, and the type of road access to the crest of the dam.

2.1.4 Accelerometers

The accelerometer that yielded the highest and most consistent frequency response in the Phase I equipment tests was chosen for recording seismic data on the dry surfaces of concrete dams. Specifications and a diagram of the accelerometer are included in appendix A. This accelerometer is very small, measuring only 0.55 inches (14.0 mm) long. Two thin wires are soldered directly to pins on the top of the accelerometer housing.

Because of the small accelerometer size and fragile cabling, the accelerometers were stud-mounted inside plastic geophone cases for field use (figure 2-11). A hole was drilled in the base of each geophone case, through which a male-female standoff was placed and secured internally with a lock washer and nut (figure 2-11a). The male ends of the standoffs, which project into the centers of the geophone cases, were tapped and threaded to accept the integral stud on the accelerometer housing. The female ends of the standoffs project out of the base of the geophone cases and are sized to thread onto 1/4-inch male concrete anchors installed on the concrete dam surface. The delicate accelerometer wires are spliced onto thicker wires, which are surrounded by a durable jacket and strain-relieved as they exit the geophone case (figures 2-11b and 2-11c). The jacketed cable from each geophone case is about 2 feet long, with a 3-pin connector on the end. These connectors attach to a custom-built multi-conductor cable that has 16 takeouts spaced 2 feet apart (figure 2-11d). Extension cables may be used to allow a different accelerometer spacing.

(a) (b)

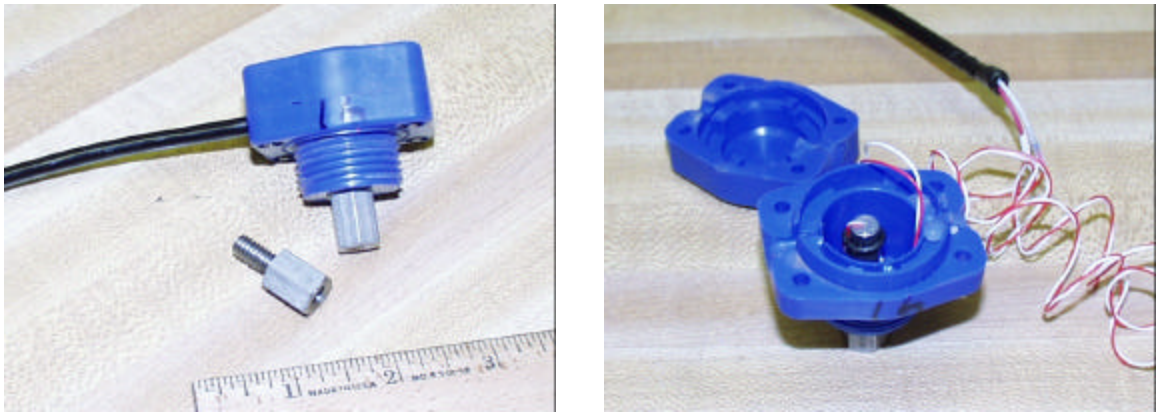

(c) (d)

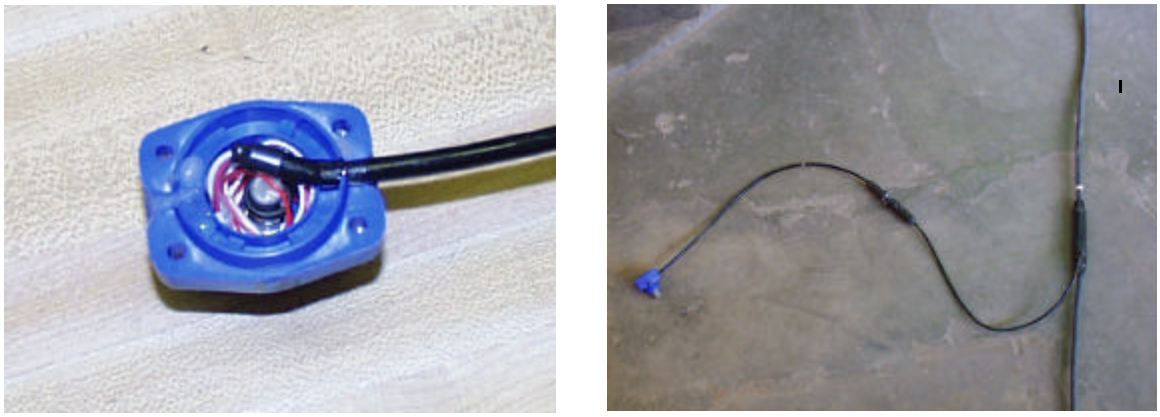

FIGURE 2-11: Accelerometer mounted in geophone case. (a) Side view showing male-female standoff. (b) View of accelerometer inside case. (c) Top view showing strain relief of cable as it exits the side of the case. (d) Accelerometer attached to the take-out cable.

2.1.5 Accelerometer Amplifier Box

Electronics to power the accelerometers and amplify the signals were constructed and enclosed in the box shown in figure 2-12a (designed and built by Matrix-5 Technologies, Inc.). This box attaches to the top of the accelerometer take-out cable. A jumper cable going to the recording system attaches to the opposite side of the box. These electronics receive power through the jumper cable, either directly from the custom-designed recording system described in section 2.1.6 below, or from two external 12-volt batteries if an alternate recording system is used. The electronics distribute power to each accelerometer. In addition, this box contains an amplifier board for each of the 16 accelerometer channels. (See appendix A for the amplifier specifications.) The amplifier gain for each channel is individually controlled by the size of the resistor installed on the board for that channel (figure 2-12b). These resistors are attached with thumb screws and can be easily changed to vary the amplifier gain. The maximum gain is 33 dB.

The accelerometer electronics generally performed well in the field. The only problem noted is a slight bias on the output signals. If high amplifier and digitizer gains are used, the output signals

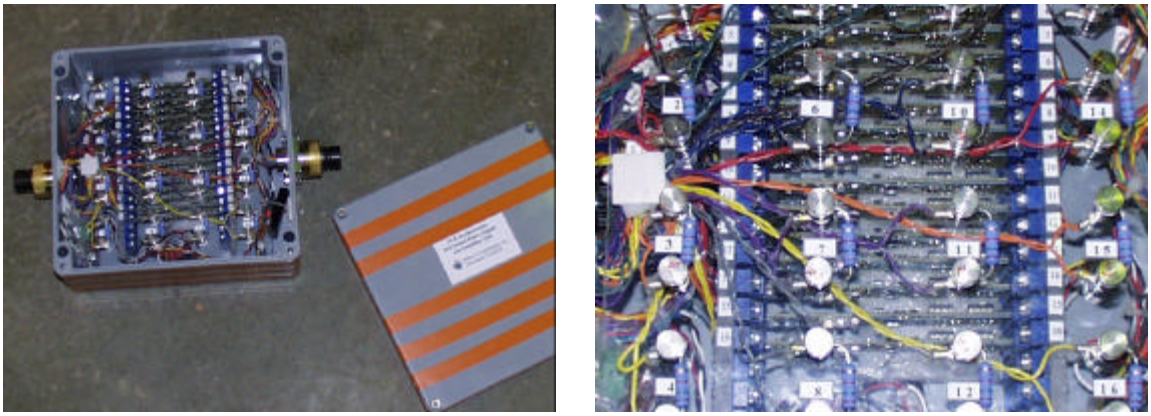

FIGURE 2-12: (a) Accelerometer amplifier box. (b) Close-up view of amplifier electronics, showing resistors used to adjust amplifier gains.

may be shifted outside the input range for the recording system, resulting in a severely clipped recorded signal. This may be avoided by carefully selecting the gains.

2.1.6 Seismic Recording System

Because frequencies up to 16 kHz were obtained during the Phase I tests conducted at Monticello Dam (Block, 1998), a multichannel recording system was built specifically for recording high-frequency seismic data on concrete structures. While a standard industry seismograph could have been used, it is considered only marginally acceptable for frequencies in this range. The new recording system was designed by Matrix-5 Technologies, Inc. This system can record data from as many as 20 channels simultaneously, at a base sampling interval of 12.5 μsec . (Longer sampling intervals may be specified if desired). Each channel has a 16-bit digitizer and programmable gain control. The maximum signal input voltage is from -10 volts to +10 volts. The maximum number of samples per channel is 225,000, equivalent to a record length of 2.81 seconds at the base sampling interval. Additional specifications of this acquisition system are included in appendix A.

Data acquisition is controlled by a DOS-based computer program that has a menu-driven user interface. This software is used to specify the active channels and to set source and receiver locations, the sampling interval, record length, and pre-trigger time. The digitizer gains may be set manually with this program, or they may be set automatically using the amplitudes from the last set of data to compute new gains. After each source impact, the data from all active channels are uploaded simultaneously from the digitizers to the computer via a high-speed bus. All traces are displayed on the monitor screen as soon as the upload is complete. If desired, the data may be automatically filtered before it is displayed, using a filter designed by the operator. Data from multiple source impacts may also be stacked to improve the signal-to-noise ratio. The stacking may be done automatically, or the data from each impact may be previewed before either being accepted and stacked or rejected. In preview mode, the waveforms from the new hit are overlaid on the previously-stacked waveforms for comparison. When stacking is complete, all stacked traces may be saved in a single file on the hard drive in SEG-2 32-bit fixed point format. Source and/or receiver locations may be changed between source impacts using previously-specified increments,

(a)

(b)

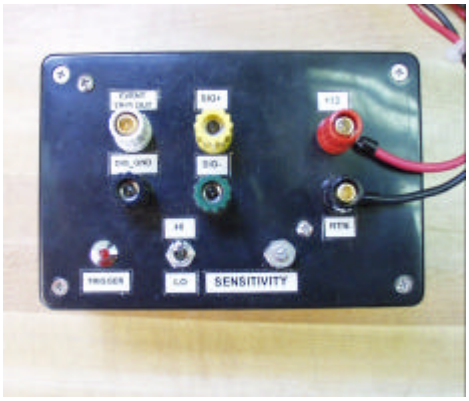

FIGURE 2-13: (a) Recording system rack-mounted in shockproof cases. The upper case contains the power supply and computer. The lower case contains the digitizer boxes. The bus is mounted in the back of the lower case (not shown). (b) External trigger box for the recording system.

or the locations may be changed manually.

The recording system requires conditioned AC power. A power supply distributes power to the digitizers, as well as to the hydrophone or accelerometer amplifiers.

The digitizers, computer, power supply, and bus are rack-mounted in two portable shockproof plastic cases (figure 2-13a). An external computer monitor and keyboard must be attached to the system on site. An external trigger box is also required (figure 2-13b). This box converts an analog signal from a trigger (such as an accelerometer signal or an electrical contact closure signal) into a digital signal that triggers the recording system. Triggering occurs when the trigger input signal changes by a certain level, in either the positive or negative direction. The sensitivity level of the triggering is adjusted manually using switches on the trigger box.

2.1.7 Cables

The following cables were built for use with the seismic tomography equipment:

• Three jumper cables to go between the seismic recording system and either the hydrophone string or the accelerometer amplifier box. Cable lengths are: 300 feet, 600 feet, and 10 feet (test cable).

• An accelerometer take-out cable. This cable has 16 take-outs spaced 2 feet apart.

• Eight 20-foot extension cables for use with the accelerometer take-out cable. These cables may be used to allow an accelerometer spacing other than 2 feet. At Seminoe Dam, the extension cables were used to simultaneously record data from accelerometers mounted across the dam crest and accelerometers mounted on the upstream face.

• Two trigger cables on reels. Each cable is between 250 and 300 feet long. Each trigger cable may be used with either the electrical contact closure trigger (on the nail gun) or the accelerometer trigger (on the sledge hammer).

• Two power cables that may be used to feed power to either the hydrophone string or the accelerometer amplifier box. These cables are needed only if the custom-designed recording system described in section 2.1.6 is not used. They are designed to be used with any of the three standard geophysical industry seismographs currently owned by Reclamation.

• Two cables for the electrical contact closure trigger used on the nail gun source.

2.2 Software Developments

Some computer software was developed during this research project specifically for use in seismic tomography surveys on concrete structures, while other existing software was modified for this application. Two software packages are described in this section. The first program, SYNSEIS, was developed during this project for designing a tomography survey with optimum data acquisition geometries. The second program, PIKSEIS, was developed by Reclamation a few years ago for other seismic data applications and was extensively modified under this project for use in seismic tomography data processing. PIKSEIS is used to process geometry information and seismic waveform data and to display tomographic images. A separate in-house program is used to perform the tomographic inversion. That program was not modified significantly under this project and is not described here.

2.2.1 Survey Design Software: SYNSEIS

While design of typical cross-borehole tomography surveys is simple and straightforward, design of surveys across structures with more complex geometries can be difficult. To obtain good spatial resolution of the images from a tomography survey, data must be acquired with the proper source-receiver geometries. Ideally, data should be acquired for as wide a range of ray angles (angle of the ray path between the source and receiver) as possible. Limitations caused by time constraints in the field, radiation patterns of sources and receivers, and the geometry of the structure under investigation nearly always prevent complete ray coverage in geophysical tomography. Proper survey design can help obtain the best coverage possible within the limitations present.

SYNSEIS is a computer program that was developed for design of seismic tomography surveys. It is written in Interactive Data Language (IDL), a licensed graphics and mathematical software development package, and it can only run on a computer with a current IDL license. It has a menu-driven user interface and runs under the Windows operating system. SYNSEIS uses Windows'

printer/plotter drivers for hardcopy output. Alternatively, output can be sent to a computer file (postscript, CGM, HP-GL, or PCL format). While much of the code can handle three-dimensional geometries, the program has only been used and tested for designing two-dimensional surveys.

SYNSEIS allows the user to interactively design a data acquisition geometry and then examine images indicating how much ray coverage each part of the dam (or other structure under investigation) receives for that geometry. The user can then adjust the acquisition geometry until the desired ray coverage is achieved. The program builds an ascii file that concisely describes the acquisition geometry designed by the user. A print-out of this file can be used in the field as a guide during data acquisition. The user can examine this file to determine the total number of source impacts that the acquisition geometry requires. This aids in estimating the amount of time it will take to complete the survey and the quantity of field supplies that are needed. The major features of this program are described in more detail below.

MAJOR FEATURES:

• Defining the Coordinate System

The program uses a right-handed coordinate system with the "z" axis pointing upward. The user specifies the azimuth of the "x" axis.

• Defining the Project Geometry

Geometry elements along which sources and receivers are to be placed may be defined in three ways:

1. using borehole deviation files - measurements of cable depth, inclination, and azimuth. SYNSEIS computes "x" ,"y", and "z" coordinates from these input data.

2. using line survey files - coordinates of points along a profile. The coordinates may be given as "x", "y" , and "z" values, or they may be given as distance and azimuth from the coordinate system origin and elevation. In the latter case, SYNSEIS computes "x" and "y" values from the input distances and azimuths.

3. manually inputting coordinates of individual point source and receiver locations.

Using line survey files containing "x", "y", and "z" values is the most common approach. Inputting coordinates of individual source or receiver locations is generally inefficient, and some options used in designing the survey are not available when data are input in this manner. The description of features described below assumes that only boreholes or line surveys are used. All geometry elements defined for a project may be plotted in plan or vertical view, and hardcopy output may be obtained.

• Designing a survey

The survey is designed in a way that mimics the manner in which the data are acquired in the field. When seismic tomography data are acquired, the survey is typically performed in the following manner. An array of receivers, normally with an equal receiver spacing, is fixed in a given location. Data are then recorded for multiple source locations. These source locations are

usually equally spaced along a survey line (such as across the dam crest or along the downstream face), and data are acquired sequentially along the survey line. A set of data acquired with a fixed receiver array and a sequential set of source locations is referred to as a sweep. Another sweep may then be acquired by placing the sources along a different survey line or by moving the receiver array. The survey is designed in SYNSEIS by creating multiple sweeps. For each sweep, the following information is entered independently for the source and receiver locations:

- name of the geometry element on which the sources or receivers are placed (chosen from a drop-down list of all borehole and line survey names in the project)
- distance along the geometry element of the first source or receiver
- source or receiver spacing
- number of receivers or maximum number of source locations
- maximum angle from the source or receiver axis (which is assumed to be perpendicular to the geometry element) for which ray paths may be created. This option is used to avoid ray paths for which sufficient energy cannot be generated or recorded because of source or receiver radiation patterns.

In addition, a maximum ray angle from horizontal may be specified. This option is used simply to limit the number of ray paths based on data acquisition time constraints or the desired level of spatial resolution. The distance along the geometry element of the first source and the number of source locations specified by the user are automatically adjusted by the program, based on the ray angle restrictions imposed.

Each sweep may be displayed, either alone or in conjunction with any other specified sweep. An example of a sweep created during the survey design for Seminoe Dam is shown in figure 2-14.

Sweep definitions created in SYNSEIS are saved in an ascii computer file. This file may be printed and used in the field to guide data acquisition. An example of a sweep ascii file is shown in figure 2-15, with annotations describing the entries.

• Computing the Ray Coverage

Several parameters relating to the ray coverage achieved with the designed survey may be computed and displayed. All parameters are computed by dividing the area under investigation (the area bounded by all defined geometry elements) into cubes of a specified size. The ray coverage parameters are then computed for each cube, using all ray paths that pass through it. SYNSEIS does not import velocity models or perform curved ray tracing, and therefore all ray paths are assumed to be straight for these calculations. The following parameters are computed :

1. the number of hits, i.e., the number of rays passing through the cube
2. the angle from horizontal of the steepest up-going ray (degrees)
3. the angle from horizontal of the steepest down-going ray (degrees)

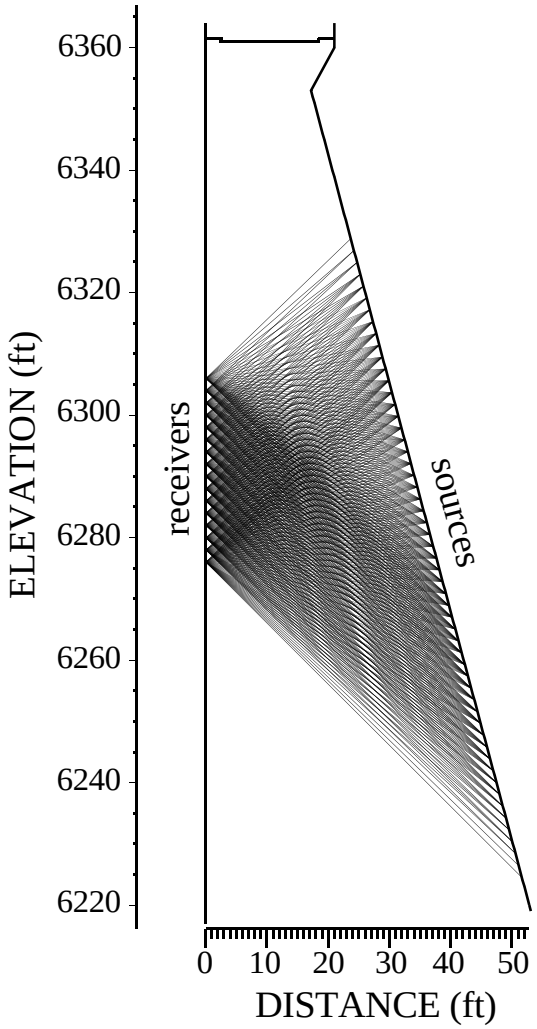

FIGURE 2-14: Example of a sweep designed and plotted using SYNSEIS. There are 16 receivers along the upstream dam face, and 55 source locations along the downstream face.

4. the angle between the steepest up-going ray and the steepest down-going ray (degrees, equal to #2 + #3).

The last three parameters are illustrated in figure 2-16. Parameters 2, 3, and 4 are described above for a vertical cross section. Computations for these three parameters are actually performed independently for the x-z, y-z, and x-y planes (within each cube). Currently, however, only the computations computed for the vertical x-z plane are output to the hard drive. A computer file is generated for each of the four parameters listed above. Each file contains the results for all cubes. The results may be plotted as color-coded images. Examples of these images are presented in figure 2-17.

14 (number of sweeps)

REC_NAME	REC_D1	REC_INC	NO_REC	RECANG_MAX	SRC_NAME	SRC_D1	SRC_INC	NO_SRC	SRCANG_MAX	ANG_MAX
ACC	4.00000	2.00000	8	90.0000	DS	3.00000	2.00000	27	90.0000	90.0000
ACC	23.9300	2.00000	5	70.0000	DS	3.00000	2.00000	27	70.0000	90.0000
ACC	23.9300	2.00000	5	70.0000	ACC	5.00000	2.00000	7	70.0000	90.0000
ACC	23.9300	2.00000	5	90.0000	ACC	2.00000	2.00000	1	90.0000	90.0000
ACC	23.9300	2.00000	5	90.0000	ACC	20.0000	2.00000	1	90.0000	90.0000
HYDRO	14.0000	2.00000	16	90.0000	ACC	20.0000	2.00000	1	90.0000	90.0000
HYDRO	14.0000	2.00000	16	90.0000	ACC	2.00000	2.00000	1	90.0000	90.0000
HYDRO	14.0000	2.00000	16	90.0000	ACC	5.00000	2.00000	7	90.0000	90.0000
HYDRO	14.0000	2.00000	16	90.0000	DS	3.00000	2.00000	53	70.0000	70.0000
HYDRO	46.0000	2.00000	16	90.0000	DS	13.0000	2.00000	75	70.0000	70.0000
HYDRO	78.0000	2.00000	16	90.0000	DS	39.0000	2.00000	89	70.0000	70.0000
HYDRO	110.000	2.00000	16	90.0000	DS	43.0000	2.00000	98	70.0000	70.0000
HYDRO	142.000	2.00000	16	90.0000	DS	63.0000	2.00000	108	70.0000	70.0000
HYDRO	174.000	2.00000	16	90.0000	DS	81.0000	2.00000	98	70.0000	70.0000

LEGEND:
REC_NAME: Name of geometry element on which receivers are located
REC_D1: Distance of first receiver (ft)
REC_INC: Receiver increment, or spacing (ft)
NO_REC: Number of receivers
RECANG_MAX: Maximum ray angle from receiver axis allowed (deg)
SRC_NAME: Name of geometry element on which sources are located
SRC_D1: Distance of first source location (ft)
SRC_INC: Source increment (ft)
NO_SRC: Number of source locations
SRCANG_MAX: Maximum ray angle from source axis allowed (deg)
ANG_MAX: Maximum ray angle from horizontal allowed (deg)

FIGURE 2-15: Example of a sweep ascii file generated by SYNSEIS.

2.2.2 Waveform Processing Software: PIKSEIS

An existing in-house computer program, originally written for processing crosshole shear-wave data, was extensively modified for use in seismic tomography data processing. The revised program, PIKSEIS, is used for computing source and receiver coordinates, filtering and plotting waveform data, determining arrival times and amplitudes, and exporting data files needed for input into external tomographic inversion software. The images, or tomograms, from the tomographic inversion can be imported into PIKSEIS and displayed as color-coded images with the outline of the dam (or other geometry elements) superimposed.

Like SYNSEIS, PIKSEIS is written in IDL, runs under the Windows operating system, and has a menu-driven user interface. Hardcopy output may be obtained through the Windows printer/ plotter drivers, or plots and tables can be sent to computer files (postscript, encapsulated postscript, CGM, HP-GL, or PCL format).

PIKSEIS operates in one of three specified modes, depending on the type of survey being analyzed: crosshole S-wave, downhole, or general single-component. The last mode is used for analyzing typical seismic tomography data. The major features of PIKSEIS operating in this mode are described below.

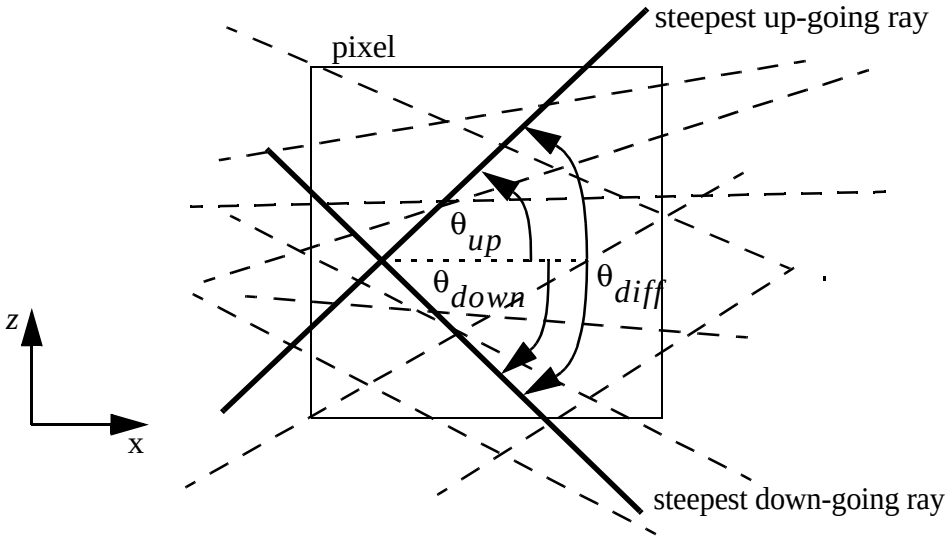

LEGEND:

θ_{up}	angle from horizontal of the steepest up-going ray
θ_{down}	angle from horizontal of the steepest down-going ray
θ_{diff}	angle between the steepest up-going ray and the steepest down-going ray

FIGURE 2-16: Three of the ray coverage parameters computed by SYNSEIS.

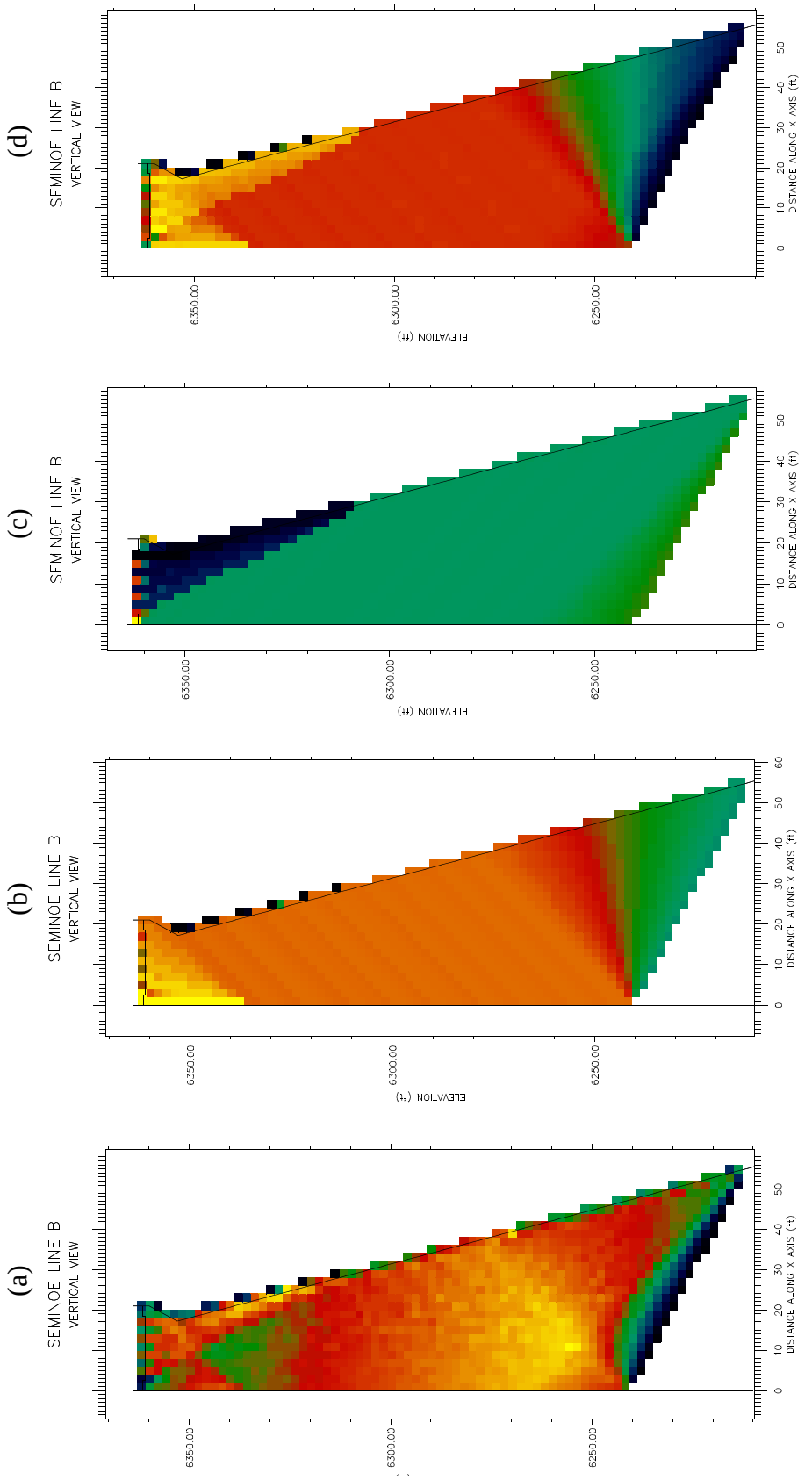

FIGURE 2-17: Examples of ray coverage images plotted in SYNSEIS: (a) number of hits, (b) angle from horizontal of the steepest up-going ray, (c) angle from horizontal of the steepest down-going ray, (d) angle between the steepest up-going ray and the steepest down-going ray

MAJOR FEATURES:

• Defining the Coordinate System

The program uses a right-handed coordinate system with the "z" axis pointing upward. The user specifies the azimuth of the "x" axis.

• Defining the Project Geometry

Geometry elements are defined in the same manner as described above for SYNSEIS, using borehole deviation files, line surveys, or point source/receiver locations.

• Defining the Survey Layout

An input dialog is provided for entering information related to data acquisition. This information includes specifying which channel contains the trigger trace (if any), how many polarities were acquired, and how the source and receiver geometry elements are to be determined for each trace (i.e., how to determine on which geometry element the source is located and on which geometry element the receiver is located). The source and receiver geometry elements may be determined in several ways, including using a single LINE_ID variable in each trace header (this assumes that the source and receiver are on the same geometry element), using separate SOURCE_LINEID and RECEIVER_LINEID variables in the trace header (this method was used for the survey conducted at Seminoe Dam), or creating a list of either data filename numbers or the last characters in the data filenames and corresponding source and receiver geometry element names.

• Creating an Index File of All Traces in the Data Set

PIKSEIS scans the headers of all seismic data files in a specified data directory and builds an index file containing the following information for each trace:

- the filename prefix of the data file
- the trace channel number
- source identifier, consisting of the source geometry element name and the source distance
- receiver identifier, consisting of the receiver geometry element name and the receiver distance
- receiver component name (for single-component tomography data, the "TR" component name indicates the trigger traces, and the "REC" component name indicates all other receiver traces)
- source polarity (not relevant for single-polarity P-wave data)
- type of source (e.g., "hammer" or "nail gun")
- type of receiver (e.g., "hydrophone" or "accelerometer")

Columns are also included for the arrival times and corresponding arrival time pick weights and the computed amplitudes (described below). The index file may be edited, either within PIKSEIS or externally, to modify any parameters that were saved incorrectly in the file headers during data acquisition or to delete unwanted traces.

• Computing Source and Receiver Locations

PIKSEIS creates files containing the source and receiver Cartesian coordinates. For each trace in the index file, PIKSEIS interpolates the source and receiver "x", "y", and "z" coordinates based on the source and receiver distances and the coordinates of the source and receiver geometry elements.

• Computing the Ray Coverage

The same ray coverage parameters that are computed within SYNSEIS (see section 2.2.1) may be computed and displayed within PIKSEIS. This allows the user to examine the ray coverage that was achieved during data acquisition. (All traces in the index file are used in computing the ray coverage, and straight ray paths are assumed.)

• Filtering Waveforms

Waveforms may be filtered using a low-pass, high-pass, band-pass, or band-stop filter. The filters are zero-phase and are applied in the frequency domain by multiplying the magnitude spectrum by a user-defined window with Hanning tapers. The user may choose to filter the raw data or may apply a new filter to previously filtered traces. A filter may be tested initially on data from a single file. During this test, the original and filtered traces are overlaid on the screen so that the user may evaluate the effectiveness of the filter. The user may alter the filter until the desired results are obtained and then automatically apply the final filter to all data files. The filtered data are written in new files on the hard drive.

• Plotting Waveforms

The waveform data can be plotted in several formats, including plotting traces from an individual file, a source or receiver gather, a common offset section (all traces having a specified difference in source and receiver distances), a common dip section (traces from ray paths having a specified dip from source to receiver), or a vertical section (traces from horizontal ray paths only, plotted as a function of elevation). The user selects the type of data to plot, including selecting raw or filtered traces and specifying desired components and polarities. The appearance of the plot can be altered in numerous ways, including specifying the amplitude scaling of the waveforms (normalized or true amplitude); specifying the degree of waveform smoothing (running-average smoother); correcting the times using previously determined trigger times; displaying arrival time picks; specifying colors of the background, axes, and waveforms; and specifying the line thickness. The ranges of the "x" and "y" axes can be explicitly altered, or the user can create a zoom window to plot a subset of the data. A figure caption can be added, and hardcopy output can be sent directly to a printer or to a computer file.

• Determining Arrival Times

The program can automatically determine first-break arrival times using the amplitude ratios

of data within two moving windows (a forward window and a backward window). The user can then use the plotting capabilities described above to view and manually edit the time picks. Large amounts of data can be rapidly scanned by paging through source or receiver gathers. (The user may manually pick the arrival times without performing the auto-picking first, if preferred.)

• Computing Arrival Time Pick Weights

Arrival time pick weights can be computed within PIKSEIS. These weights are included in the exported tomography pick file (described below) and are used in the external tomographic inversion software to weight the arrival times. These pick weights indicate the relative accuracy of the arrival times based on waveform signal-to-noise levels. The arrival time pick weight is given by:

$$weight = (foramp)/(backamp).$$

Foramp is a measure of the signal level, given by the amplitude of the first waveform peak or trough (depending on the polarity) after the arrival time pick. *Backamp* is a measure of the noise level, given by the median absolute amplitude value in a window of user-specified length before the arrival time pick. Mathematically, these variables are expressed by:

$$foramp = max(abs(dataf - bias))$$

and

$$backamp = median(abs(datab - bias))$$

where *dataf* is a vector of the data values in the forward window (consisting of the first half-cycle of the waveform after the time pick), *datab* is a vector of the data values in the backward window, and *bias* is the waveform bias, or offset. Currently, a maximum pick weight of 100 is allowed. (Larger values are truncated when the tomography pick file is exported.)

• Computing Amplitudes

Amplitudes can be automatically computed for all traces after the first-break arrival times have been determined. Amplitudes are computed within a time window beginning at the arrival time on each trace and having a user-specified length. The user must select one of three available types of amplitude values to compute:

- Peak-to-peak amplitude (max(*data*)- min(*data*))
- Average absolute amplitude (mean(abs(*data*))
- Median absolute amplitude (median(abs(*data*))

(Data is a vector containing the data values within the specified time window). The user must also specify whether to perform the calculations on the raw data or on filtered data (if filtering has been performed) and may specify different window lengths or types of amplitude calculations for different components, if desired.

• Computing Frequency Spectra

PIKSEIS contains a limited feature for computing and plotting frequency spectra of seismic arrivals. This feature can be applied only after the first-break arrival times have been determined.

Using the arrival time and a user-defined window length, the seismic arrival is extracted from each waveform using a Hanning window. A fast Fourier transform (FFT) is performed on these extracted data. All traces from one specified data file are processed. Currently, only the magnitude spectra are displayed. These spectra are plotted on the screen sequentially (like a gather of seismic traces). The plotting options described previously are available, including the ability to zoom around a single spectrum. The plot may be sent to a printer or saved in a computer file. The frequency spectra values are not written to the hard drive.

• Exporting Tomography Files

A feature is available for exporting data files that are used as input to a customized, in-house seismic tomography inversion program. Three files are exported, including a time pick file, a source location file, and a receiver location file. Information in these data files includes: source and receiver identifiers, source and receiver coordinates, arrival times and corresponding pick weights, amplitudes, source and receiver types, and variables indicating whether any source or receiver coordinates or time corrections will vary during the tomographic inversion. Before export, the arrival times may be corrected using the trigger times, if desired, or the trigger times may be output in the source location file as source time corrections.

• Plotting Tomograms

After the tomographic inversion has been performed, the resulting velocity (or attenuation) model can be imported into PIKSEIS and displayed as a color-coded image. Geometry elements are overlaid on this image (such as the outline of the dam). Options are available for changing the color map and velocity scale, zooming, adding a figure caption, and obtaining hardcopy output.

3.0 PHASE III - FIELD TESTS AT SEMINOE DAM

The effectiveness of the seismic tomography method, as applied to concrete structures, has been evaluated by acquiring and processing seismic tomography data from Seminoe Dam, Wyoming. This structure was chosen for the field tests for several reasons. Most importantly, the concrete in Seminoe Dam is undergoing alkali aggregate reaction (AAR). This chemical reaction causes expansion of the concrete and a corresponding decrease in P-wave velocity (Swamy and Wan, 1993; Thomas et al., 1995). Because of earlier field examinations of Seminoe Dam and concrete core analyses, the extent of concrete deterioration within Seminoe Dam was anticipated to be extensive enough to provide targets (P-wave velocity variations) within the spatial resolution of the ray-based seismic tomography method. In addition, at the time of these field tests, Seminoe Dam was under active investigation by the Bureau of Reclamation. Data from other investigations, including analysis of concrete core recovered in 1998, fracture mapping, and deformation studies, would be available for comparison to the seismic tomography results.

3.1 Seminoe Dam

Seminoe Dam is located on the North Platte River, approximately 31 miles northeast of Rawlins, Wyoming. It is a concrete arch dam with a structural height of 295 feet and crest length of 530 feet (figure 3-1). The maximum width at the base is 85 feet. The minimum width is 17.4 feet, at approximately 8 feet below the elevation of the crest road. The face-to-face width at the crest is 21 feet. The upstream face is vertical, and the dam is thicker at the abutments than at the crown of the arch.

Seminoe Dam was completed in 1939. The construction of the dam is described in several articles and Reclamation reports (Keener, 1937; Peugh, 1937; Seminoe Dam Construction Advances with River Diversion Completed, 1937; Warner, 1937; Rippon, 1939; Peugh, 1939; Tarleton, 1939; Warner, 1939; Huber, 1942). The dam was constructed in ten radial blocks, generally 50 feet wide, using 5-foot lifts. Modified portland cement was used with the following mix ratios by weight: water-to-cement: 0.54, aggregate-to-cement: 9.61, and coarse aggregate-to-sand: 2.4. The aggregate was acquired from the river bed 2 1/2 to 4 miles upstream from the dam, and the maximum aggregate size was 6 inches. The concrete in the dam was placed during one construction season.

Evidence of alkali aggregate reaction within Seminoe Dam was first documented in 1951 (Ramaley, 1951; Failor, 1961). Petrographic examinations of cores from holes drilled from the dam crest in 1974, 1979-1980, and 1998 confirm this finding and show that the concrete deterioration has progressed over time (Bechtold, 1975; Bechtold, 1980; Hurcomb, 1998; Hurcomb, 1999). For the core recovered in 1974, evidence of alkali-aggregate reaction was severe in the upper 5 feet, less pronounced from 5 to 20 feet, and not observed below a depth of 20 feet (Bechtold, 1975). “Appreciable alkali-aggregate reaction” was noted throughout the 78-foot cores retrieved in 1979-80 (Bechtold, 1980). Core recovered in 1998 shows significant concrete deterioration to a depth of 18 feet. The deterioration is ascribed mainly to alkali-aggregate reaction,with minor freeze-thaw damage (Hurcomb, 1998). Less severe evidence of alkali-aggregate reaction was found from 18 feet to the bottom of the 50-foot cores. The alkali-aggregate reaction

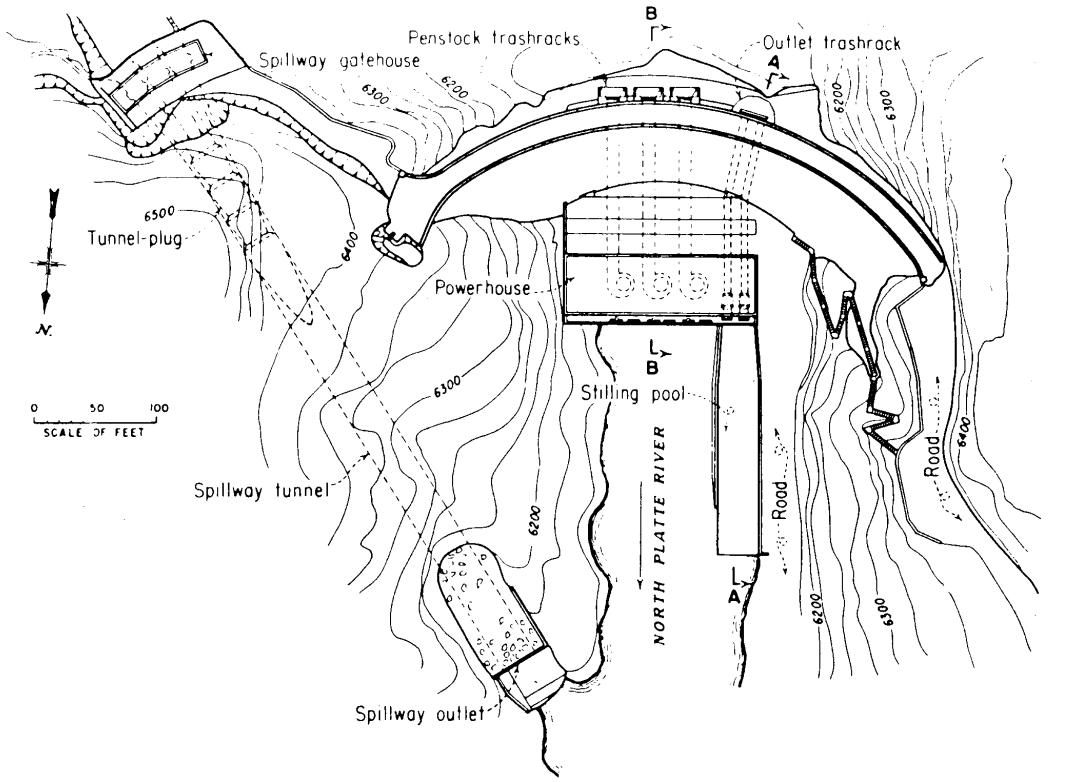

FIGURE 3-1: Plan view of Seminoe Dam, Wyoming.

within Seminoe Dam is believed to be primarily a chemical reaction between the high-alkali cement and strained quartz within coarse quartzite aggregate (Hurcomb, 1998; Hurcomb, 1999). Some chert and glassy volcanics may also contribute to the reaction. This type of AAR is more specifically referred to as alkali-silica reaction (ASR).

Mohorovic and Dolen (1999) summarize results from destructively tested core samples taken in 1979-1980 and 1998. They conclude that the concrete deterioration has caused the compressive strength and modulus of elasticity to progressively decrease with time. The average compressive strength measured on core samples taken in 1998 from the upper 50 feet of the dam is 3,580 lb/in^2 , 58 percent of the projected ultimate concrete strength, and the average modulus of elasticity is 1.72 x 10^6 lb/in^2, only 38 percent of the projected ultimate value. The 1998 average values of compressive strength and modulus of elasticity are 23 percent and 16 percent, respectively, lower than the average values measured from cores taken in 1979-1980. Morohovic and Dolen also observe that, while the degree of deterioration and strength loss decrease with depth, the rate of deterioration between 1980 and 1998 increases with depth.

Visual evidence of concrete deterioration on the surface of the dam includes cracking, spalling, and calcium carbonate deposits. Approximate locations of major cracks on the downstream face and lift lines showing staining from calcium carbonate deposits are shown in figure 3-2. Photographs of the downstream face, taken between 1996 and 1999 (Mares, 2000a), were used to locate the cracks and stained lift lines.

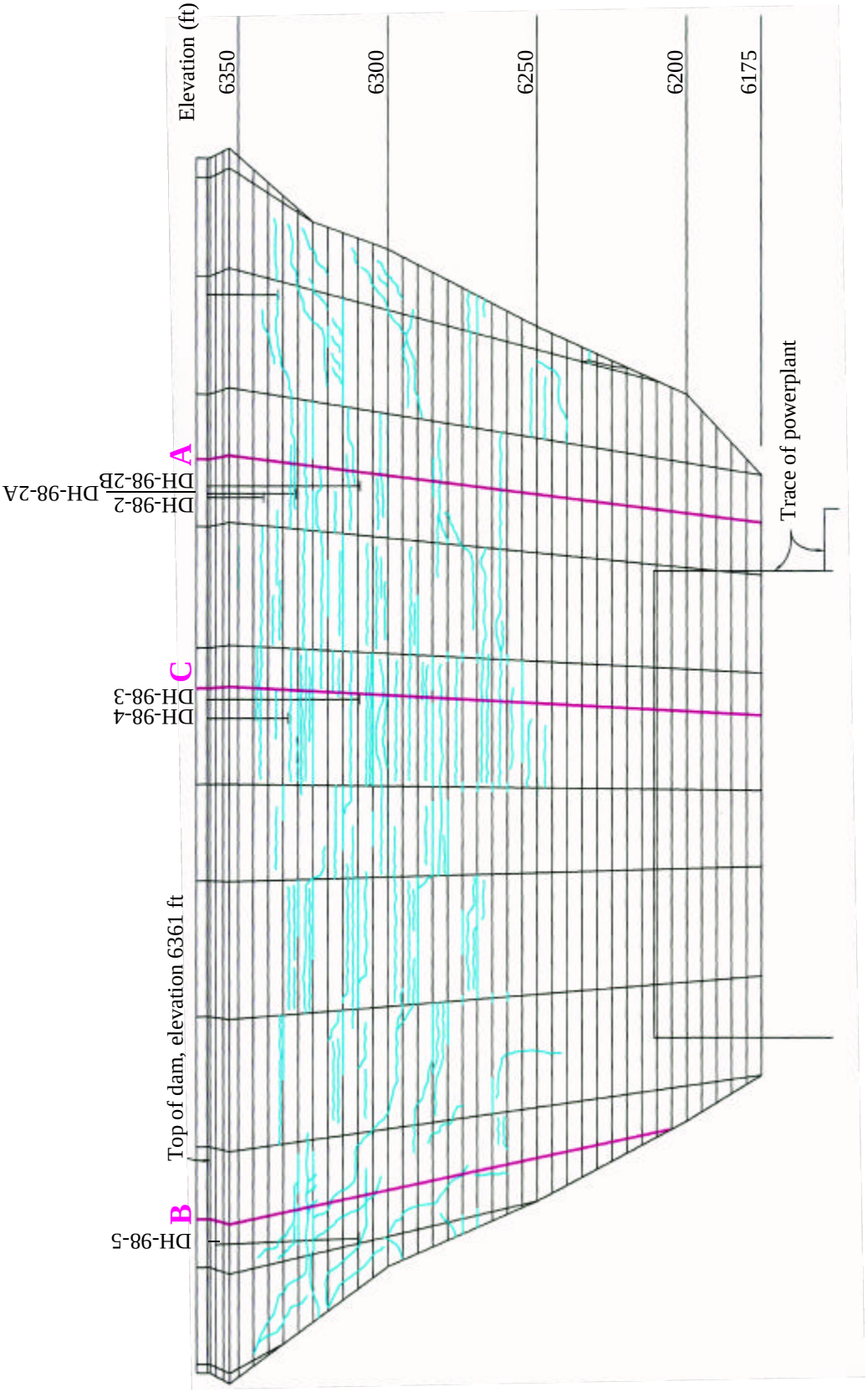

FIGURE 3-2: Major cracks and calcium-carbonate-stained lift lines on the downstream face of Seminoe Dam. This figure is based on a figure from Mares (2000a). The magenta lines and letters represent the locations of the seismic tomography cross sections.

Tomography Cross Section	Dam Station	Position Relative to Borehole	Dates of Tomography Survey	Approx. Reservoir Elevation During Survey (ft)
A	2+18	8 ft left of DH-98-2B	8/15-16/00	6350.7
B	5+03	10 ft left of DH-98-5	4/19-21/99 9/29/99	6338.8 6351.7
C	3+04	3 ft left of DH-98-3	8/18/00	6350.5

TABLE 3-1: Locations and survey dates of the seismic tomography cross sections. Reservoir elevations shown were interpolated from measurements made every 2 to 4 weeks.

3.2 Data Acquisition

Seismic data were acquired across three upstream-downstream cross sections (sections A, B, and C, figure 3-2 and table 3-1). The locations of these seismic tomography cross sections were selected to coincide with deep (50-foot) core holes from the 1998 coring program (boreholes DH-98-2B, -3, and -5, figure 3-2).

The seismic tomography data were acquired in 1999 and 2000. Data were initially collected on section B in April 1999, using the nail gun seismic source. Because of problems with the piezoelectric transducer triggers used during this trip (see section 2.1.1 for details), a second trip was required to collect additional data. Data were acquired on section B using improved triggering methods in September 1999. Half of the new data was acquired using the nail gun seismic source instrumented with an electrical contact closure trigger, and the other half of the data was acquired using a 2-lb sledge hammer source with an attached accelerometer trigger. Both seismic sources and triggering methods worked well during this trip. Data were acquired along sections A and C in August 2000. A mechanical problem with the nail gun source developed almost immediately during this field trip (see section 2.1.1). Because of time constraints, this problem was not resolved. Rather, the sledge hammer was used as the seismic source for all data acquired on sections A and C. Photographs taken during the field trips are included in appendix B.

For each tomography cross section, seismic waveforms were acquired with three source-receiver geometries: sources on the dam crest and receivers on the upstream face (or in the reservoir immediately upstream from the face), sources on the downstream face and receivers on the crest, and sources on the downstream face and receivers on the upstream face (or in the reservoir) (figure 3-3). Accelerometers, mounted on concrete anchors, were used as the receivers on the dam crest and upstream dam face above the water. Below the water, the hydrophone string, hung vertically from the crest immediately upstream from the dam, was used to record the signals. Receiver spacings on the upstream face were 2 feet, while those across the dam crest were 2 to 2.5 feet. Source spacings ranged from 2 to 3 feet. The larger spacing was used for the lowest section

FIGURE 3-3: Types of acquisition geometries used at Seminoe Dam. Each line represents a seismic ray path between a source and a receiver: (a) sources on the crest and receivers on the upstream face, (b) sources on the downstream face and receivers on the crest, (c) sources on the downstream face and receivers on the upstream face.

of the dam, where less spatial resolution is needed. Multiple depth positions of the hydrophone string were used to acquire data to the bottom of the reservoir on sections A and C. Data were acquired to a lesser depth on section B because the right abutment projects into the reservoir at that location. Seismic ray paths ranging from horizontal to approximately 70 degrees from horizontal were obtained through most of each cross section.

Data quality is extremely good, with excellent signal-to-noise ratio on most seismic traces. Nearly 2,400 high-quality waveforms were obtained for section B, while 5,600 to 5,700 good waveforms were acquired for each of the two deeper sections, A and C. Examples of typical waveforms are shown in figure 3-4.

The locations of the sources and receivers were determined as accurately as reasonably possible. To compute accurate source coordinates, the downstream face of the dam along each tomography cross section was surveyed using a total station surveying instrument. Coordinates of source and receiver locations across the dam crest and along the upstream face above the water were computed from manual measurements. Footage on the hydrophone cable was labeled for depth control. A small weight (7 to 8 lbs) attached to the end of the hydrophone string proved inadequate for preventing lateral drift of the hydrophone string during data acquisition along section B in 1999. (Data acquired with the lowest hydrophone string position on section B were omitted from the data analysis because of uncertainty in the hydrophone string position.) In 2000, a heavily-weighted positioning line (described in section 2.1.3) was used to limit lateral hydrophone drift during data acquisition along sections A and C.

3.3 Data Processing

The P-wave arrival times were used to compute a two-dimensional P-wave velocity distribution (tomogram) within each tomography cross section. A ray-based tomography inversion method was used. The forward problem included curved ray tracing, and the inverse problem was formulated as an iteratively-weighted least squares matrix inversion that approximates an L1 norm solution. A mathematical description of the inversion method is included in appendix C.

3.4 Tomography Results

The seismic tomography data acquired at Seminoe Dam clearly indicate the presence of strong lateral P-wave velocity variations. The P-wave arrival time data cannot be satisfied using homogeneous (constant-velocity) or layered P-wave velocity models. Figure 3-5 shows histograms of the arrival time residuals (differences between the observed arrival times and the corresponding arrival times computed from a given velocity model) for the best-fitting homogeneous, layered, and two-dimensional P-wave velocity models for the data acquired on section C. The mean absolute residual for the two-dimensional model is 70 percent lower than that for the layered model and 90 percent lower than that for the best-fitting homogeneous model. Furthermore, only the two-dimensional model yields residuals that are mostly within the estimated average arrival time uncertainty of about 0.05 msec. Residual distributions for sections A and B are similar to those for section C.

The P-wave velocity tomograms for the three cross sections are very similar (figure 3-6). All cross sections show very large velocity variations, ranging from as much as 16,000 ft/s to less than 7,000 ft/s. The lowest velocities occur in the upper 30 to 40 feet of the dam, as well as along the downstream face above approximate elevation 6250 feet. The areas with the lowest P-wave velocities are interpreted as regions with the most severely deteriorated concrete.

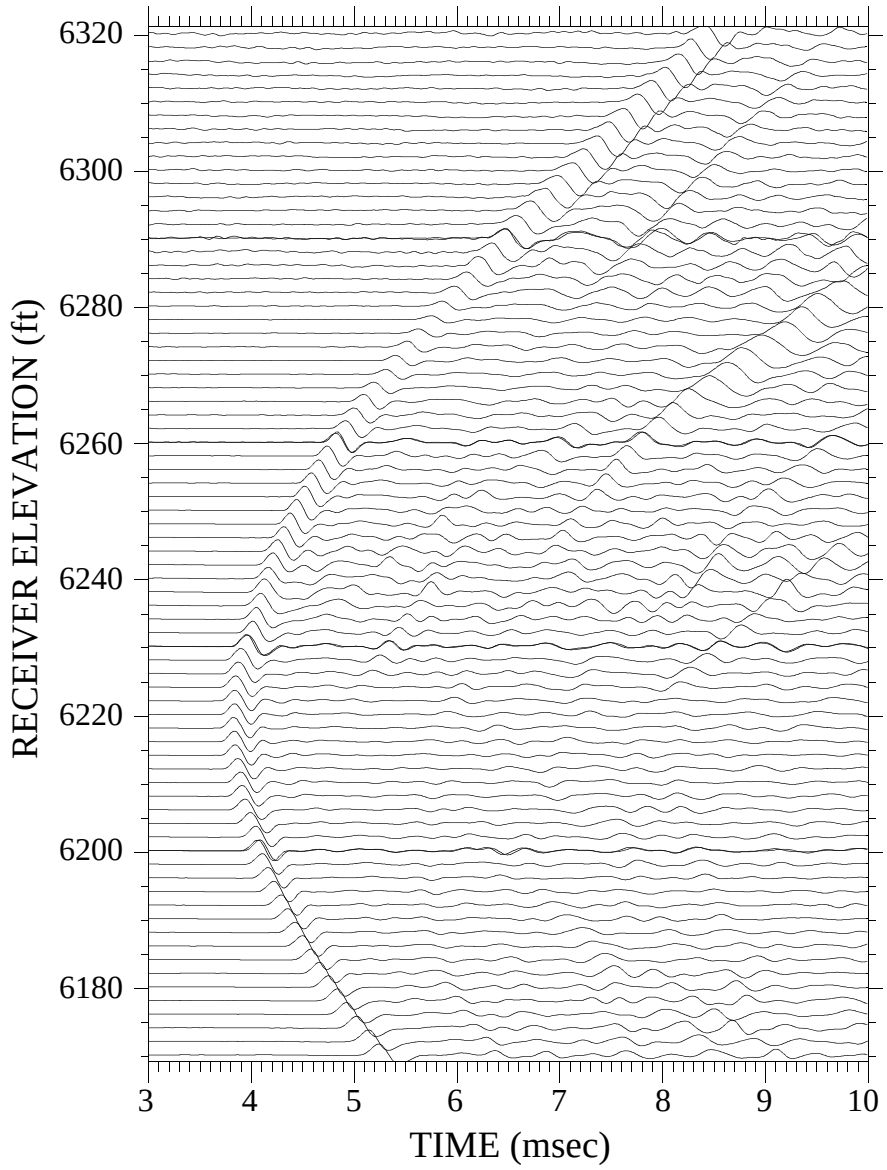

FIGURE 3-4: Examples of waveforms acquired at Seminoe Dam. Data from five positions of the hydrophone string are shown, with a common source location on the downstream face at elevation 6219 ft. The hydrophone positions overlap by one receiver spacing, so that two traces are acquired at the same elevation for 2 consecutive hydrophone string positions.

The pattern of P-wave velocity variations seen in the tomograms is consistent with other observations relating to the relative degree of concrete deterioration within the dam. Petrographic analysis and destructive testing of concrete cores consistently show that the degree of alkali aggregate reaction and freeze-thaw damage and corresponding decrease in material strength are most severe in the uppermost section of the dam and lessen with depth (Bechtold, 1975; Bechtold, 1980; Hurcomb, 1998; Mohorovic and Dolen, 1999). An elevation survey of the dam crest con-

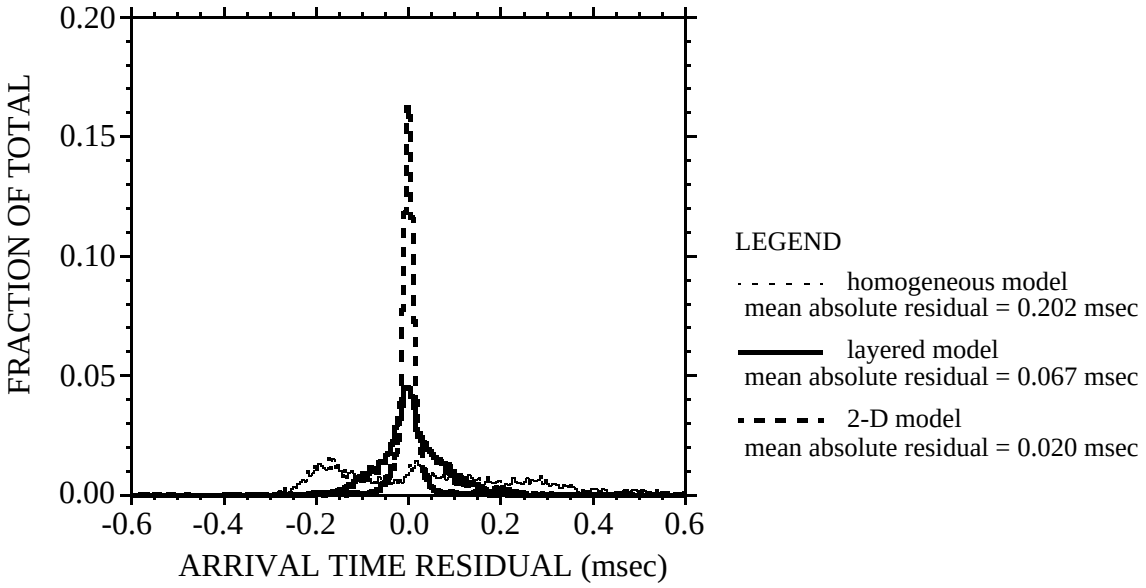

FIGURE 3-5: Comparison of the arrival time residuals for the data from section C for the best-fitting homogeneous, layered, and two-dimensional P-wave velocity models.

ducted in April 2000 indicates that the downstream side of the dam has expanded more than the upstream side (Mares, 2000b), suggesting that more severe or more extensive alkali-aggregate reaction has occurred within the downstream section of the dam than the upstream section. The above observations are consistent with the general pattern of relatively low P-wave velocities in the uppermost section of the dam and along the upper downstream face. Furthermore, many of the distinct zones with low P-wave velocities along the downstream face of the dam correlate with major mapped fractures and calcium-carbonate-stained lift lines (figure 3-6).

The low-velocity layer projecting into the dam from the downstream face between approximately 6325 and 6335 feet elevation (most distinctive on sections A and C, figure 3-6) correlates with a zone of decreased material strength measured from core samples taken during the 1998 drilling program. Values of compressive strength, modulus of elasticity, and density reported by Mohorovic and Dolen (1999) for core samples from the three boreholes near the tomography cross sections are plotted as a function of elevation in figure 3-7. (Results from samples taken from boreholes DH-98-2, -2A, and -2B are grouped together.) In general, data from all boreholes show decreased values of all three parameters at approximately the same elevations as this low-velocity layer. (Values of Poisson's ratio and failure strain measured from core samples do not show consistent trends with depth.) The velocity tomograms in figure 3-6 indicate that the concrete within this layer is most severely deteriorated on the downstream face (where the velocities are the lowest), and that the degree of deterioration decreases in the upstream direction (into the dam). This pattern may indicate that the alkali aggregate reaction within this layer began on the downstream face, where the concrete is exposed, and is progressing into the dam. Distinct low-velocity zones along the downstream face at lower elevations may represent similar patterns of

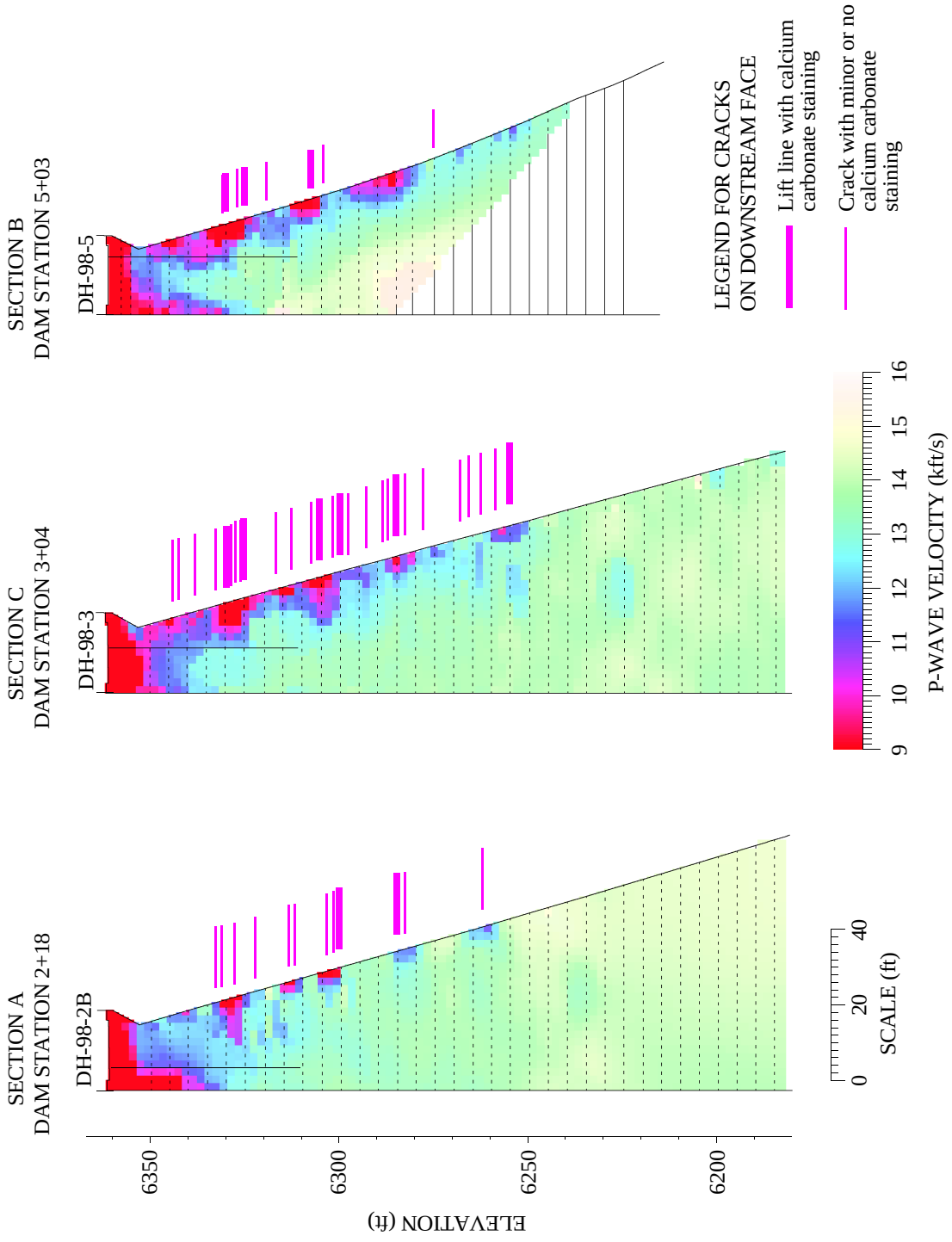

FIGURE 3-6: P-wave velocity tomograms for the three cross sections investigated.

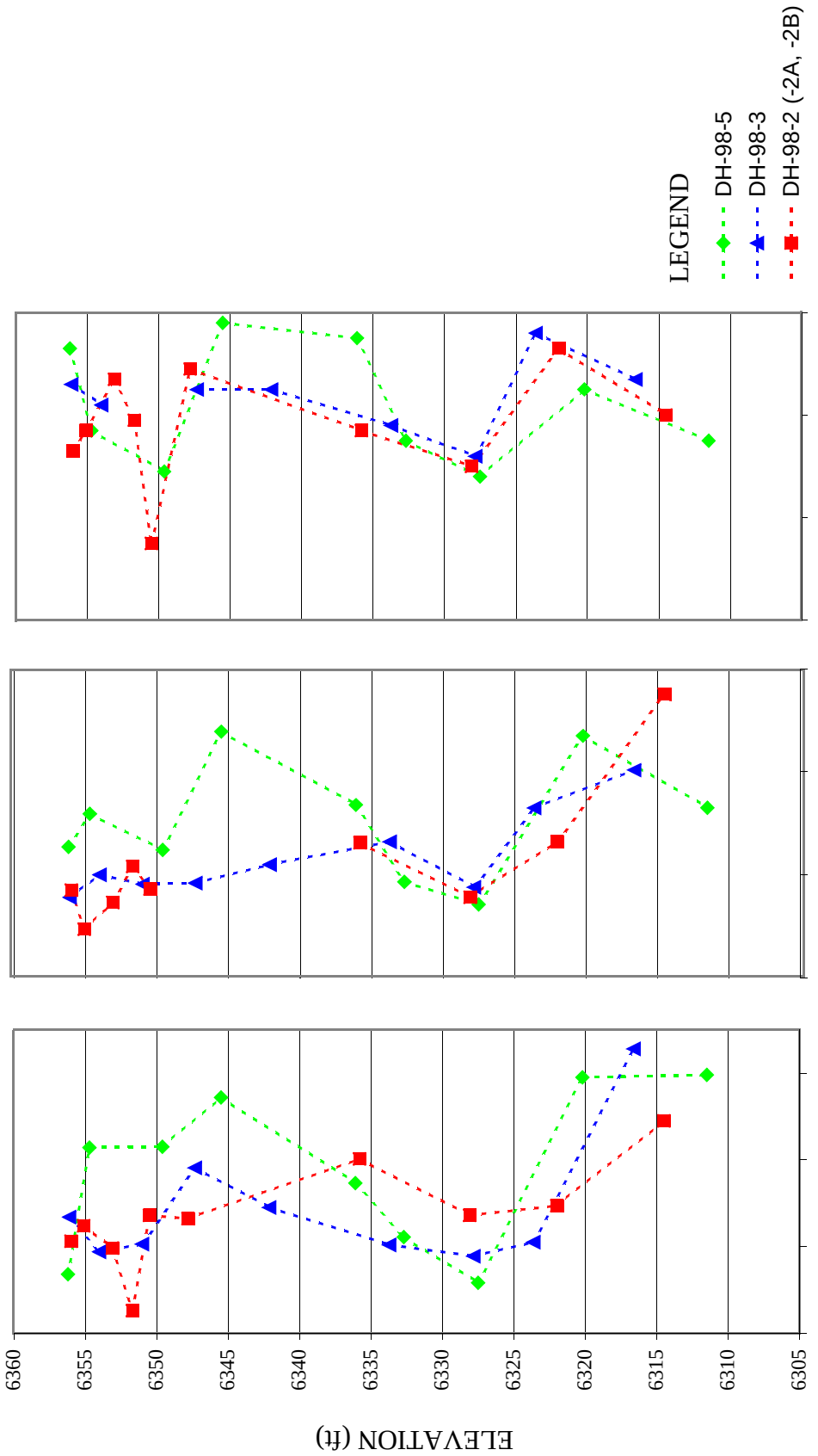

FIGURE 3-7: Compressive strength, modulus of elasticity, and density values measured from core samples from the boreholes near the tomography cross sections. These data are taken from Mohorovic and Dolen (1999).

deterioration progressing into the dam, but, to date, no boreholes have been drilled deep enough to penetrate these zones.

Although the vertical location of the low-velocity layer seen on the tomograms between elevations 6325 and 6335 feet correlates well with decreased strength, moduli, and density values measured on core samples, the lateral extent of the low-strength layer is not accurately represented by the arrival time tomography results. The low-velocity zone seen on the tomograms does not extend completely to the projected locations of the boreholes (figure 3-6), whereas the core analyses clearly indicate decreased material strength at the boreholes. Based on the core analyses, this zone of weakened concrete is judged to be thick enough to be resolved by the ray-based seismic tomography method with the frequencies recorded (generally 2 to 4 kHz), and the angular ray coverage is considered sufficient for good lateral resolution of features. The most likely reason for the apparently underestimated lateral extent of this low-strength layer in the velocity tomograms is that, beyond a certain distance from the downstream face, the velocity contrast is not sufficiently high to be detected using arrival-time tomography (because the severity of the concrete deterioration decreases away from the downstream face). The concrete cores recovered from boreholes DH-98-3 and -5 are described as intensely fractured within this zone (Mohorovic and Dolen , 1999) , and fractures were also noted in borehole image surveys at these depths within these two boreholes (Mares, 2000a). This fracturing may cause decreased material strength measurements from the core analyses, while the degree of bulk concrete deterioration is not severe enough to be accurately imaged by the seismic tomography surveys.

3.5 Correlations of P-wave Velocities and Core Measurements

P-wave velocities were extracted from the three tomograms along the projected trajectories of boreholes DH-98-2B, -3, and -5 and compared to measurements made on core samples from those boreholes. (Measurements from boreholes DH-98-2 and -2A are combined with those from borehole DH-98-2B.) Core measurements include density, Poisson's ratio, failure strain, compressive strength, and modulus of elasticity. These values were taken from Mohorovic and Dolen (1999). Scatter plots of P-wave velocity versus each of the five types of core measurements are included in figures 3-8 to 3-12. Each figure contains two plots. The upper scatter plot shows all core measurements and corresponding P-wave velocity values. The measurements from each borehole are plotted with a different symbol. The lower plot shows the measurements from all three boreholes plotted with the same symbol. In the lower plot, data points corresponding to air-dried core samples and core samples from the upper 10 feet of the dam are omitted for the following reasons. Because the dam was mostly saturated during the tomography surveys (as indicated by water seeping from the downstream face of the dam and because the vast majority of the tomography data were acquired when the reservoir was within 11 feet of the dam crest), saturated samples and samples with the in-situ moisture content preserved are believed to be much more representative of in-situ conditions than are air-dried samples. Measurements made from in-tact core samples taken from the upper 10 feet of the dam are not representative of the general concrete conditions at these depths because approximately 40 percent of the core was recovered as rubble (Mohorovic and Dolen, 1999). Because the P-wave velocities computed from the tomography data include the effect of these rubble zones and the results from the core analyses do not, the data points from these shallow depths are omitted in the lower plots in figures 3-8 to 3-12.

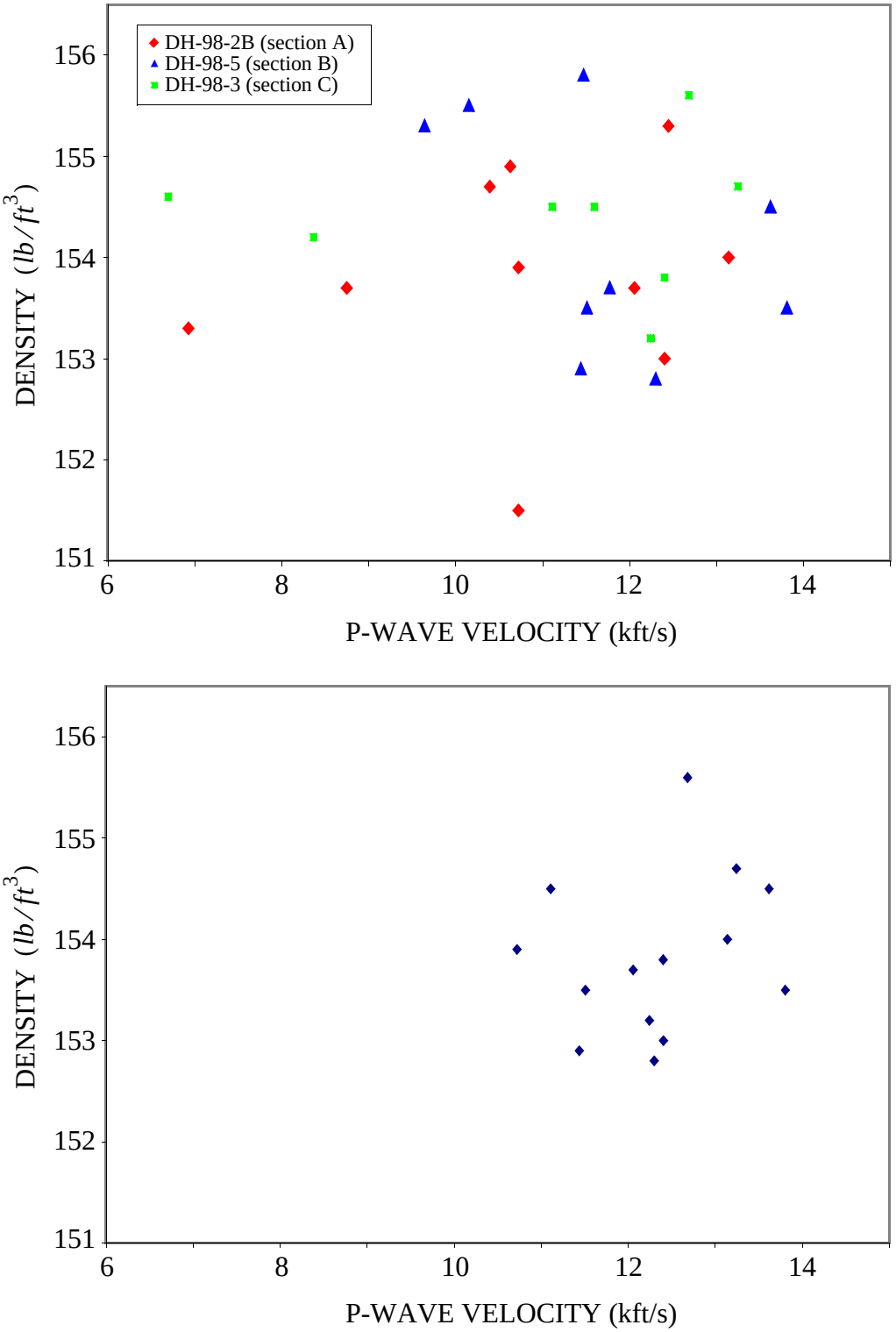

FIGURE 3-8: Comparison of P-wave velocities computed from tomography data and densities measured from core samples. See the text for an explanation of the two plots.

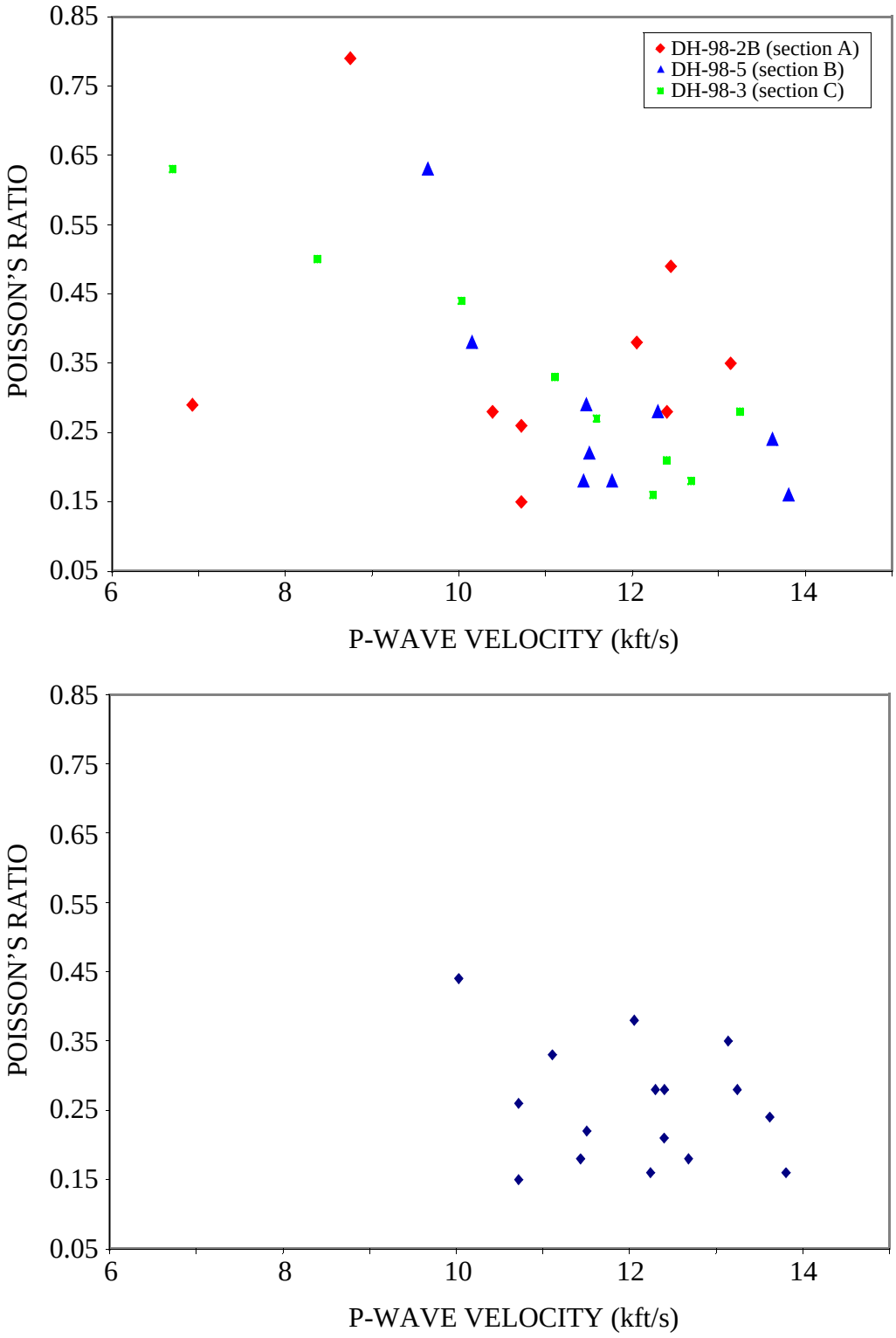

FIGURE 3-9: Comparison of P-wave velocities computed from tomography data and Poisson's ratios measured from core samples. See the text for an explanation of the two plots.

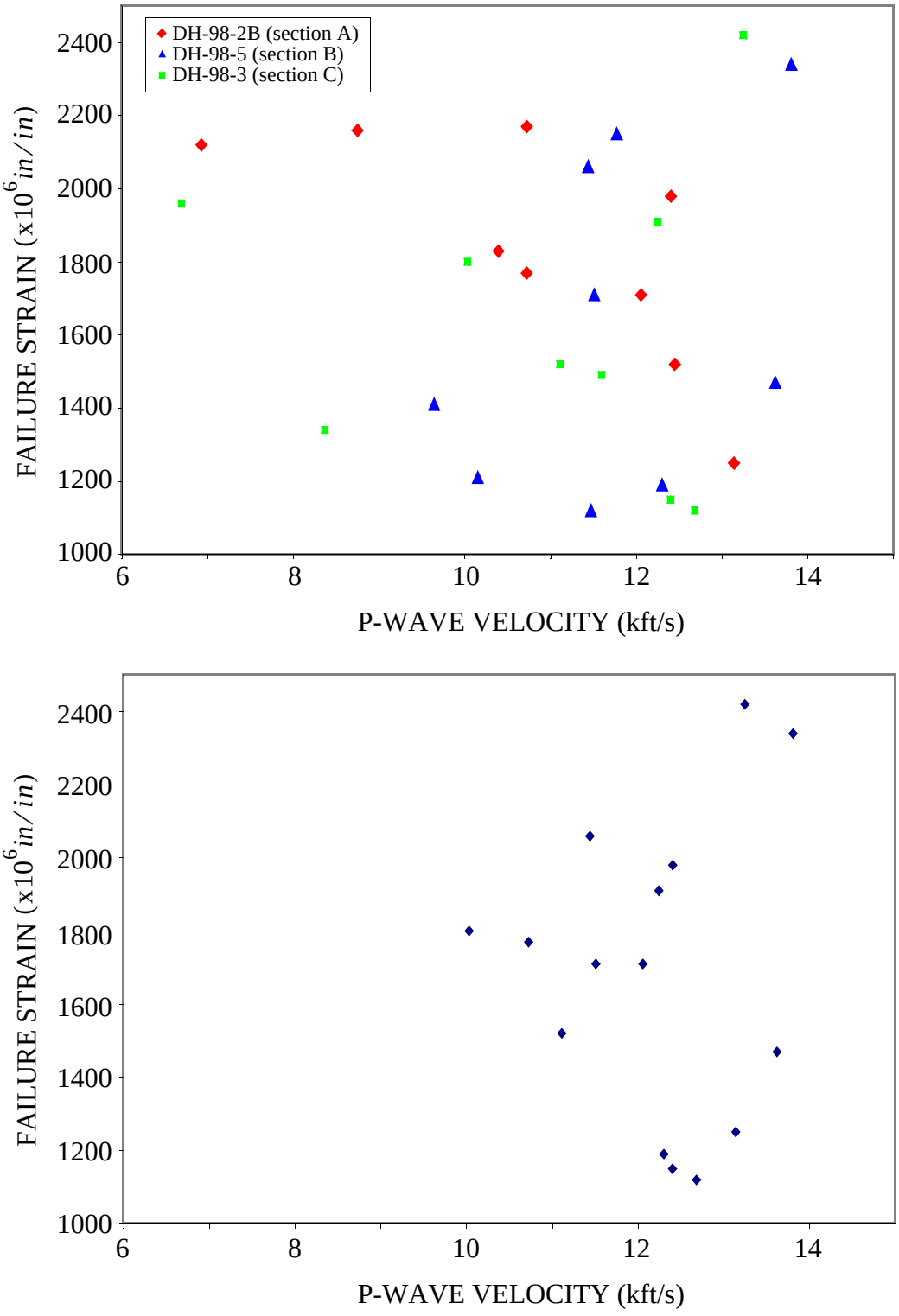

FIGURE 3-10: Comparison of P-wave velocities computed from tomography data and failure strains measured from core samples. See the text for an explanation of the two plots.

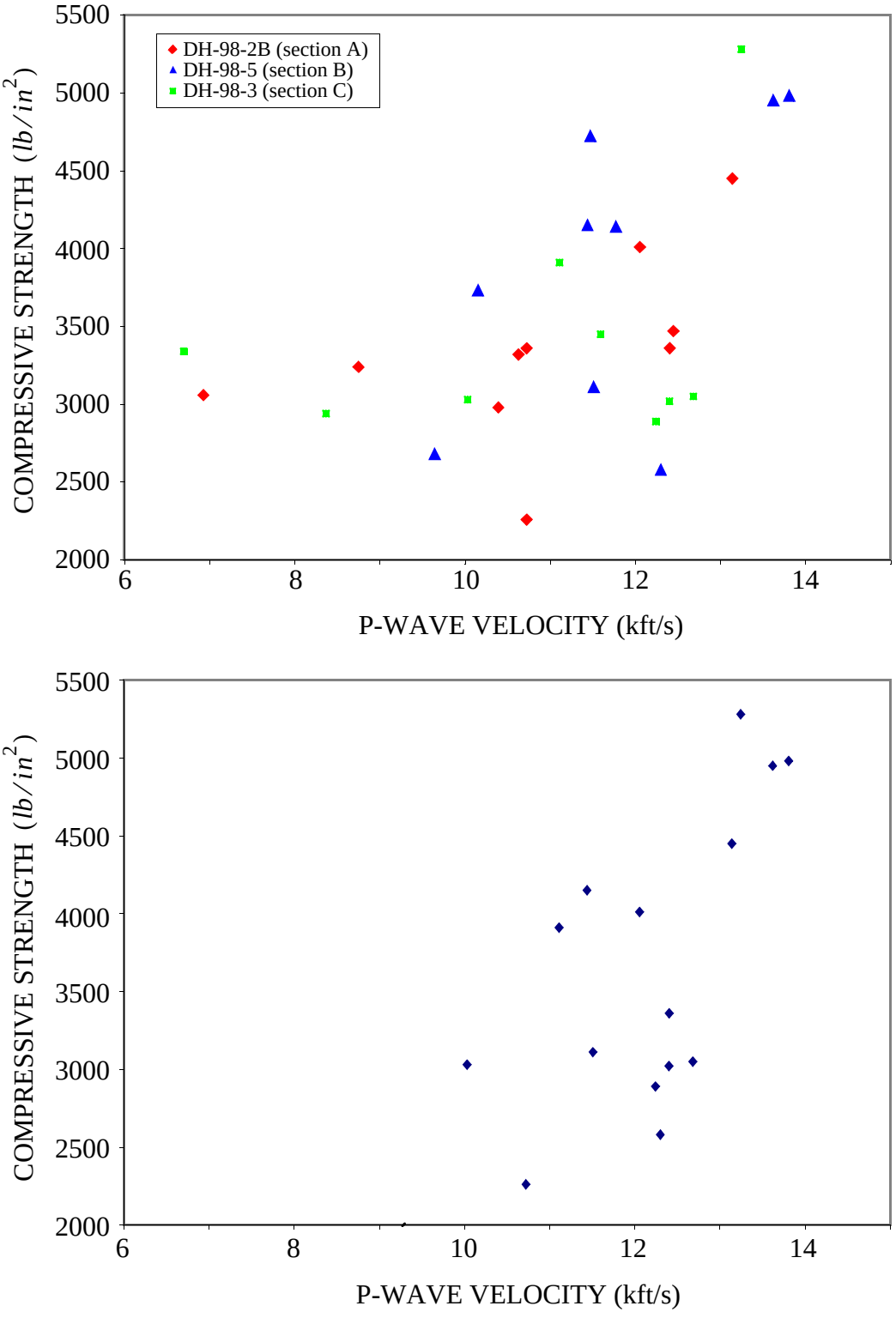

FIGURE 3-11: Comparison of P-wave velocities computed from tomography data and compressive strengths measured from core samples. See the text for an explanation of the two plots.

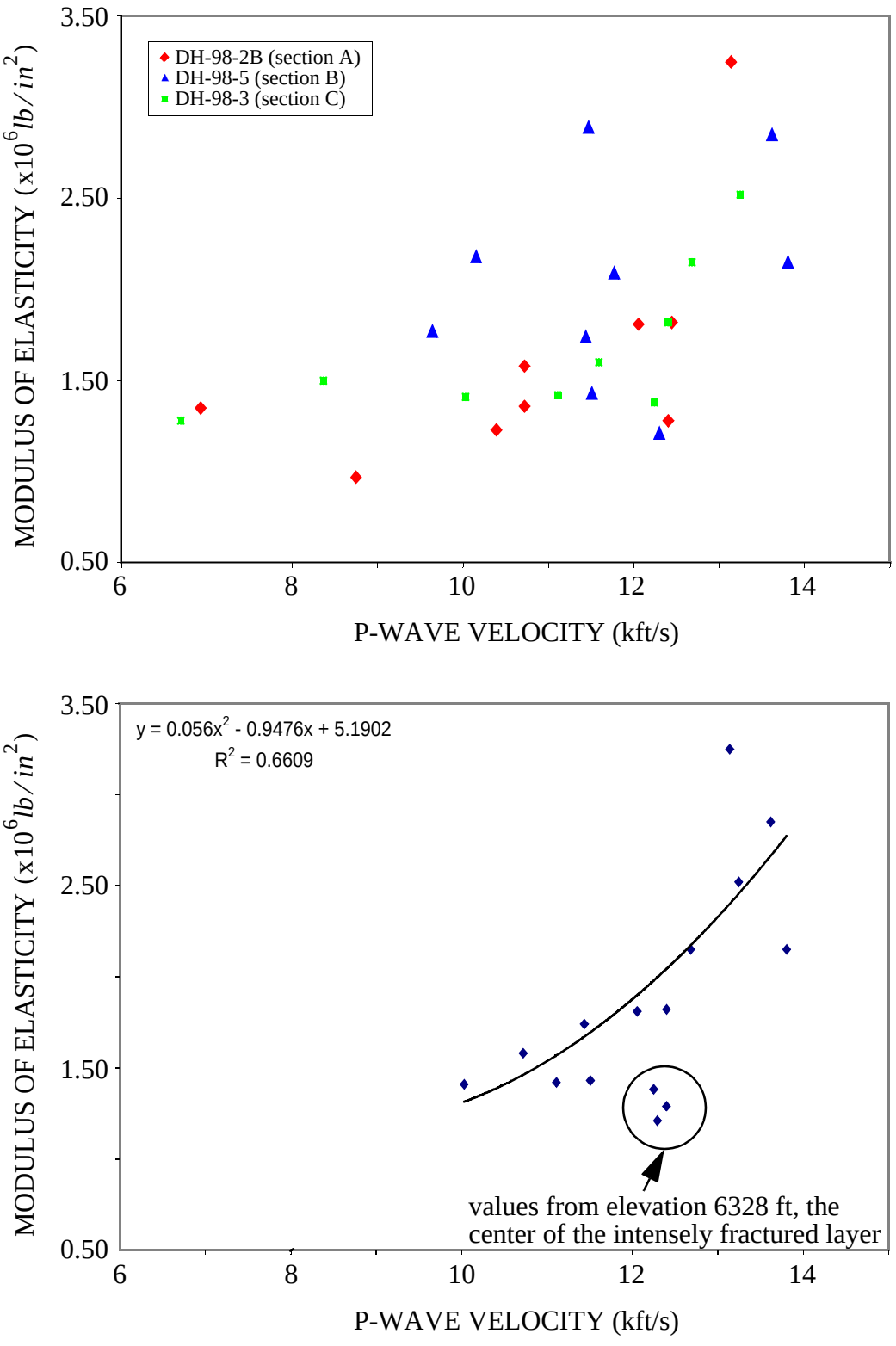

FIGURE 3-12: Comparison of P-wave velocities computed from tomography data and modulus of elasticity values measured from core samples. See the text for an explanation of the two plots.

The correlations between the P-wave velocities from the tomography surveys and the various measurements from core samples are variable. Measurements of density, Poisson's ratio, and failure strain show no correlation with P-wave velocity (figures 3-8 to 3-10). Compressive strengths generally increase with increasing P-wave velocity, although there is considerable scatter in the data (figure 3-11). The modulus of elasticity values show the most definitive correlation with P-wave velocity (figure 3-12). The modulus of elasticity values generally exhibit a nonlinear increase with increasing P-wave velocity, with the notable exception of the three circled data points in the lower plot of figure 3-12. These points correspond to core samples from approximate elevation 6328 feet, near the center of the low-strength layer discussed in detail in the previous section. As discussed previously, the core analyses appear to be more sensitive to the fracturing within this layer than are the P-wave velocities. The downward bias of these three data points in the lower plot of figure 3-12 is consistent with this hypothesis.

Omitting the three biased data points corresponding to the intensely fractured layer, a quadratic function was fit (using a least-squares norm) to the scatter plot of modulus of elasticity versus P-wave velocity (lower plot, figure 3-12). This type of function was chosen simply because it fits the observed data reasonably well. The resulting equation was then applied to the P-wave velocity tomograms to compute tomograms of modulus of elasticity. Because the empirical correlation between P-wave velocity and modulus of elasticity is only constrained in the P-wave velocity range from 10 to 14 kft/s, velocities outside this range were truncated before applying the quadratic function. The resulting tomograms of modulus of elasticity are shown in figure 3-13.

3.6 Discussion

Fracturing alone is extremely unlikely to cause the very low P-wave velocities seen along the downstream face of Seminoe Dam in the three tomography cross sections (figure 3-6). Although the locations of these low-velocity zones correlate strongly with mapped fractures on the downstream face, the very low velocities are interpreted to indicate that extensive alkali aggregate reaction is occurring in these areas. Cracking may have begun because of stresses or freeze-thaw effects. Cracking creates additional concrete surfaces that are exposed to air, water, and temperature variations, which may accelerate the alkali aggregate reaction. Expansion caused by the chemical reaction may then cause additional cracking, and the process gradually progresses into the dam.

The lack of severe concrete deterioration along the upstream face below approximate elevation 6330 feet may be largely attributed to the protective effects of the water in the reservoir. The reservoir water protects the upstream face from freeze-thaw activity and associated cracking and moderates temperature variations within the concrete. A cumulative histogram of annual minimum winter reservoir levels from 1939 to 1999 is shown in figure 3-14. The tomogram of modulus of elasticity for section A is plotted next to the histogram for comparison. For a given elevation, the histogram indicates the percentage of years for which the minimum winter reservoir level was at or below that elevation. The data indicate that the upstream dam face above elevation 6330 feet, corresponding to the area of the most severe concrete deterioration on the upstream face, has been exposed during approximately 90 percent of the winters since 1939. The histogram falls off steeply below that elevation, as does the degree of concrete deterioration on the upsteam face, as indicated by the tomograms.

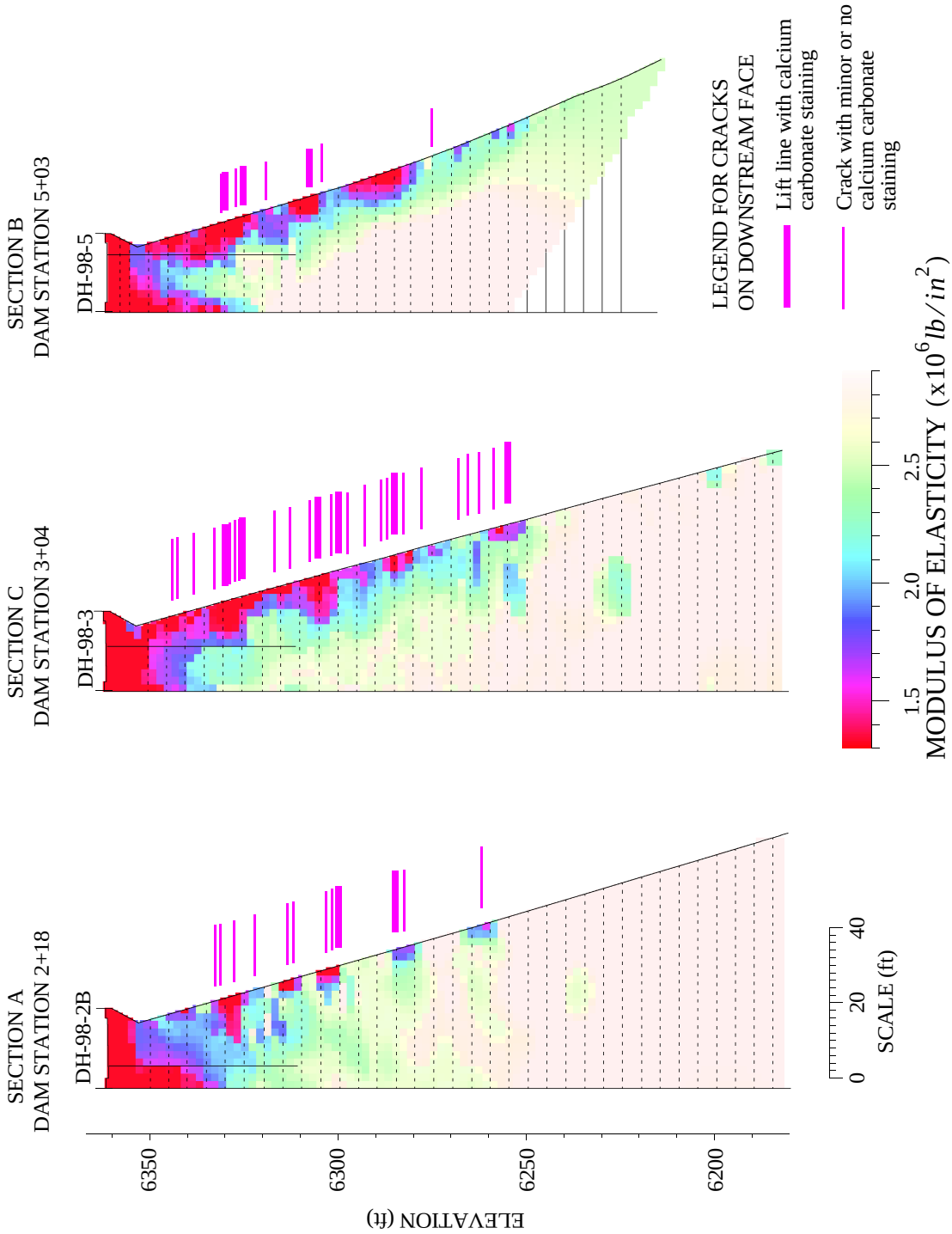

FIGURE 3-13: Modulus of elasticity tomograms for the three cross sections investigated.

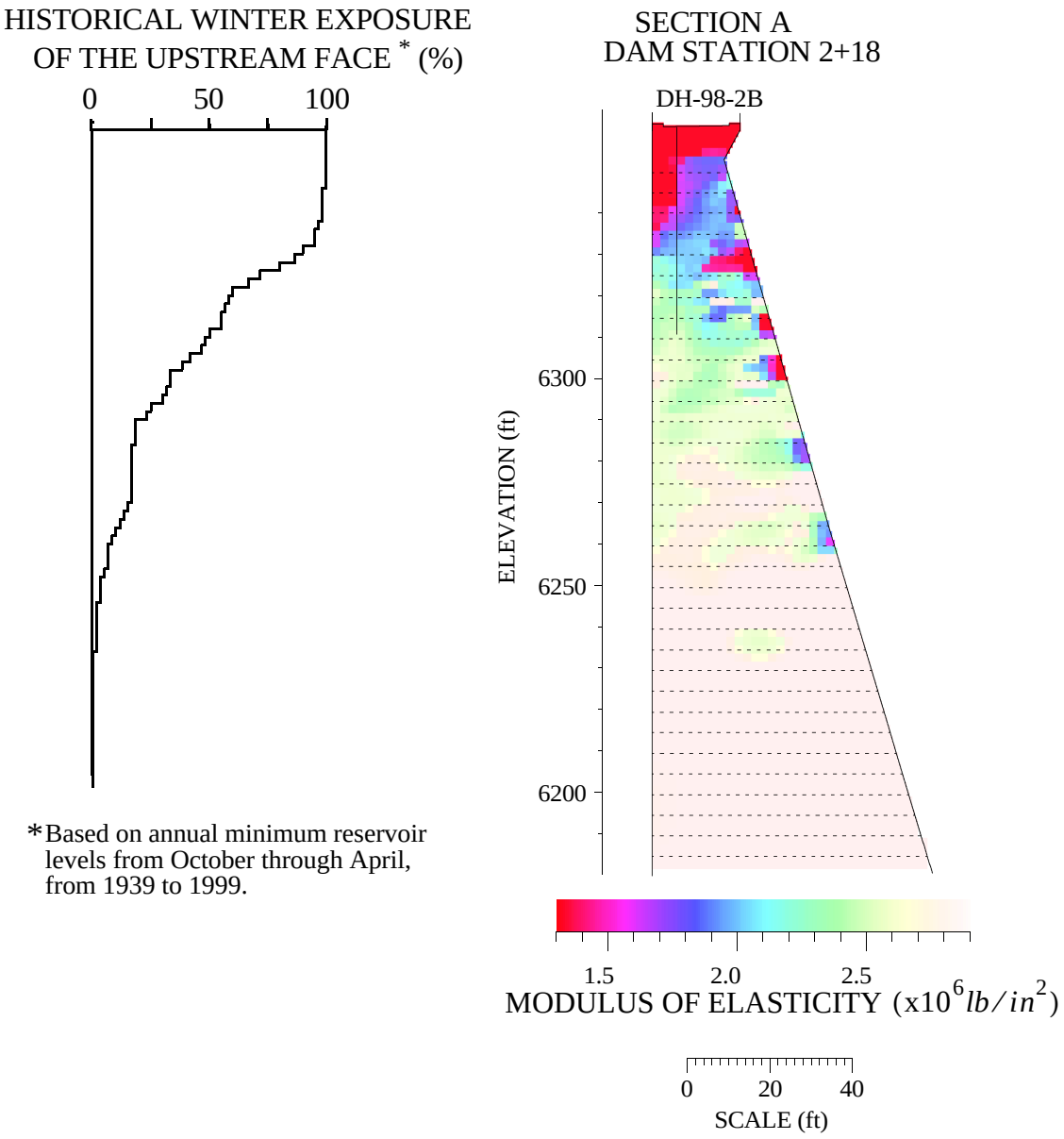

FIGURE 3-14: Cumulative histogram of annual minimum winter reservoir elevations measured between October 1 and April 30, 1939 to 1999. The modulus of elasticity tomogram for section A is included for comparison.

3.7 Conclusions

Results from the seismic tomography surveys conducted at Seminoe Dam are consistent with information obtained from core analyses, fracture mapping, and other studies and provide a more complete picture of variations of concrete properties within the dam. In addition to providing information about the current conditions within the dam, the spatial progression of concrete deterioration caused by the alkali aggregate reaction may be inferred from the images obtained from the seismic tomography surveys. Assuming that areas with the lowest P-wave velocities have undergone the highest degree of deterioration, I infer that the concrete deterioration is progressing downward from the dam crest and inward from the downstream face above elevation 6250 feet. If repeated over the course of several years, the seismic tomography method could be a useful tool for monitoring changes in the condition of the concrete within the dam.

4.0 CONCLUSIONS AND RECOMMENDATIONS

Reclamation has developed the capability of acquiring high-quality seismic tomography data on large concrete structures without drilling boreholes. Hardware and software developments achieved during this research project enable Reclamation to efficiently perform data acquisition and data processing in-house.

The seismic arrival-time tomography method may be used to image variations in concrete quality within dams and other concrete structures resulting from factors such as varying material composition, freeze-thaw damage, or alkali-aggregate reaction. Tomography surveys conducted at Seminoe Dam, Wyoming, demonstrate the usefulness of this method as applied to a concrete dam undergoing alkali-aggregate reaction. P-wave velocity tomograms computed from these surveys are consistent with information obtained from core analyses, fracture mapping, and other studies, while providing valuable additional information about the spatial progression of the concrete deterioration. Other potential applications of the method include monitoring changes in concrete quality over time and using reconnaissance tomography surveys to determine the optimum locations and depths of coreholes.

In addition to providing qualitative information about the concrete quality within dams, the results from the seismic tomography surveys can also be used in a more quantitative manner. From the correlation of modulus of elasticity values measured on core samples with the P-wave velocities from the seismic tomography surveys conducted at Seminoe Dam, tomograms of modulus of elasticity values were computed. Although the number of data points used in the correlation for Seminoe Dam was limited, the results indicate the feasibility of extrapolating core measurements away from the boreholes using results from seismic tomography surveys. Two-dimensional images of material property parameters such as modulus of elasticity values would provide engineers with much more information for computer modeling studies than can be obtained from core analyses alone.

In the future, other waveform characteristics, such as amplitude or frequency content, should be analyzed in addition to the P-wave arrival times. These waveform parameters are likely to be more sensitive than the arrival times to some types of concrete deterioration, such as fracturing, and, therefore, may detect some features that are not accurately imaged using arrival-time data alone. For example, tomographic analysis based on amplitudes or frequencies may yield a more accurate indication of the lateral extent of the zones of concrete deterioration and fracturing progressing inward from the downstream face of Seminoe Dam than the arrival time tomography results.

While face-to-face seismic tomography surveys on concrete dams provide valuable information without the necessity of drilling boreholes, tomography surveys between boreholes and the faces of a dam should also be considered, when feasible. Such surveys are likely to yield higher-resolution images than face-to-face surveys because the distances would be shorter, and, therefore, the frequencies would be higher and data could be obtained for steeper seismic ray paths.

5.0 REFERENCES

Bechtold, C. A. Petrographic Examination for Alkali-Aggregate Reaction - Seminoe Dam - North Platte River Project, Wyoming, Memorandum to Chief, Hydraulic Structures Branch, Petrographic referral code 75-2, Bureau of Reclamation, Denver, Colorado, January 20, 1975, 2 pp.

_____. Petrographic Examination of Concrete Core - Seminoe Dam - Kendrick Project, Wyoming, Memorandum to Chief, Concrete and Structural Branch, Petrographic referral code 80-46, Bureau of Reclamation, July 24, 1980, 4 pp.

Block, L. Seismic Tomgraphy of Concrete Structures, Phase I: Equipment Tests, Dam Safety Office Report DSO-98-002, Bureau of Reclamation, Denver, Colorado, September 1998, 69 pp.

_____. Seismic Tomgraphy Results from Seminoe Dam, Memorandum to Chuck Redlinger, Dam Safety Office, Bureau of Reclamation, Denver, Colorado, March 7, 2000, 3 pp.

_____. Seismic Tomography Results from Seminoe Dam, Memorandum to David Achterberg, Chief, Dam Safety Office, Bureau of Reclamation, Denver, Colorado, October 11, 2000, 3 pp.

Failor, S. V. Inspection of Seminoe Dam and Powerplant for evidence of alkali-aggregate reactivity, travel report to Assistant Commissioner and Chief Engineer, Commissioner's Office, Bureau of Reclamation, Denver, Colorado, January 16, 1961, 6 pp.

Huber, E. Final Report on Construction of Seminoe Dam and Power Plant, United States Department of the Interior, Bureau of Reclamation, Kendrick Project, Wyoming, October 1, 1942.

Hurcomb, D. R. Petrographic Examination of Concrete - Seminoe Dam - Kendrick Project, Wyoming, Memorandum to Manager, Waterways and Concrete Dams Group; Earth Sciences and Research Laboratory No. 8340-98-45, Petrographic referral code 98-20, Bureau of Reclamation, October 26, 1998, 12 pp.

_____. Petrographic Examination of Destructively Tested Concrete Core for Evidence of Alkali-Silica Reaction - Seminoe Dam - Kendrick Project, Wyoming, Memorandum to Manager, Waterways and Concrete Dams Group; Earth Sciences and Research Laboratory No. 8340-99-10, Petrographic referral code 99-05, Bureau of Reclamation, March 30, 1999, 7 pp.

Keener, K. B. Seminoe Dam I - Site Exploration and Design Studies, *Engineering News-Record*, March 18, 1937, 395-399.

Mares, D. Seminoe Dam, Report on the Preliminary Crack Survey using Photographs of the Downstream Face of Dam and Borehole Images, Bureau of Reclamation, Denver, Colorado,

March 29, 2000a, 9 pp.

_____. Seminoe Dam,Interim Report of Findings, Concrete Deterioration Issue Evaluation, Bureau of Reclamation, Denver, Colorado, October 2000b, 40 pp.

Mohorovic, C. E., and T. P. Dolen, 1998-99 Concrete Coring - Laboratory Testing Program, Seminoe Dam, Kendrick Project, WY, Bureau of Reclamation, August 1999, 29 pp.

Peugh, V. L. Seminoe Dam II - Construction Plant for Seminoe Dam, *Engineering News-Record*, March 18, 1937, 399-400.

Peugh, V. L. Contractor's System of Form Design and Concrete Placing at Seminoe Dam, *Western Construction News*, March 1939, 98-101.

Ramaley, D. Evidence of Alkali-Aggregate Reaction in Concrete Cores from Seminoe Dam - Kendrick Project, Memorandum to R. C. Mielenz; Petrographic referral code 51-28, Bureau of Reclamation, February 23, 1951, 5 pp.

Rippon, C. S. Aggregate and Concrete Production at Wyoming's Seminoe Dam Project, *Pit and Quarry*, January 1939, 52-60.

Seminoe Dam Construction Advances with River Diversion Completed, *Western Construction News*, October 1937, 407-409.

Swamy, R. N., and W. M. R. Wan. Use of Dynamic Nondestructive Test Methods to Monitor Concrete Deterioration Due to Alkali-Silica Reaction, *Cement, Concrete, and Aggregates*, vol. 15, 1993, 39-49.

Tarleton, G. Procedure in Cooling Seminoe Dam - Kendrick Project, Memorandum to Mr. K. B. Keener, Bureau of Reclamation, Denver, Colorado, May 26, 1939, 4 pp.

Thomas, M. D. A., D. Wiese, H. Caratin, and J. Stroczkowski. Ultrasound Tomography Applied to AAR-Affected Concrete Structures, *Second International Conference on Alkali-Aggregate Reactions in Hydroelectric Plants and Dams, U. S. Committee on Large Dams*, October 1995, 14 pp.

Warner, J. H. Seminoe Dam Progress, *Engineering News-Record*, November 18, 1937, 817-822.

_____. Construction of Seminoe Dam and Power Plant, Kendrick Project, Wyoming, *The Reclamation Era*, October 1939, 269-272.

APPENDIX A
HARDWARE SPECIFICATIONS

LOW-IMPEDANCE, VOLTAGE-MODE

HIGH-SHOCK ACCELEROMETER

with built-in amplifier

Series 305A

PCB PIEZOTRONICS

MOTION shock & vibration

- **rugged, light-weight, highly reliable design**
- **very high resonant frequency**
- **built-in amplifier – low impedance output**
- **no zero shift**
- **operates over long coaxial or 2-wire cables**
- **quality signal independent of cable motion or length**

For measurement of high amplitude pyrotechnic shocks associated with ballistic projectiles, metal to metal impacting, explosive forming, closed bombs and blast effects on structures.

Model 305A quartz accelerometer measures mechanical shock motion to 100 000 g. Small size and light weight impart fast response (less than 10 microseconds) and assure a minimum effect on the structure of the test object. It follows transient events up to 0.1 second duration and generates a quality signal independent of cable length, condition and motion.

This miniature transducer with an integral mounting stud installs by threading into a tapped hole in the structure of the test object. For electrical connections in extreme shock environments, the optional solder pin connector adaptor and fine stranded ribbon wire (007A Cable Assembly) has proved more durable than coaxial components.

The rigid structure of this transducer contains a very small seismic mass preloaded against a quartz element by a thin walled sleeve, mechanically isolated from the outer case. A built-in unity-gain microelectronic amplifier lowers the output impedance and improves resolution by eliminating the cable capacitance effect on amplifier noise.

When connected to a PCB power unit, self-amplifying PCB transducers generate a high-level, low-impedance analog output signal proportional to the measurand and compatible with most readout instruments. Power is supplied over the signal lead.

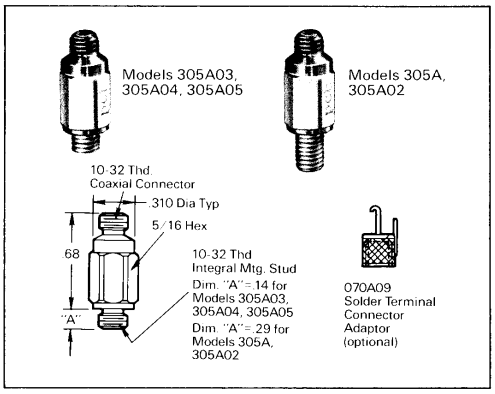

SPECIFICATIONS: Model No.		305A
Range, FS (5V output)	g	100 000(1)
Resolution	g	2.0
Sensitivity	mV/g	0.05
Resonant Frequency (mounted)	Hz	60 000
Time Rise	μs	5
Discharge Time Constant	s	2
Frequency Response (±5%)	Hz	0.25 to 8000
Frequency Response (2.5dB)	Hz	0.15 to 20 000
Linearity	%	1
Overload Recovery	μs	10
Output Impedance	ohm	<100
Transverse Sensitivity	%	5
Strain Sensitivity	g/μin/in	0.2
Temperature Coefficient	%/°F	0.03
Temperature Range	°F	-100 to +250
Vibration/Shock (max transverse)	g	75 000/30 000
Weight	gm	4.5
Excitation/Constant Current	VDC/mA	-18 to +28/2 to 20

(1) **Optional 5V Ranges**		**Model No.**
50 000 g	0.1 mV/g	305A02
10 000 g	0.5 mV/g	305A03
5000 g	1 mV/g	305A04
2500 g	2 mV/g	305A05
Charge-Mode	0.2 pC/g	315B(2)

(2) Larger Size (.47 Dia x .70 High)

To specify metric Thd M5 x 0.8, add prefix "M" to model no. – e.g. M305A

TYPICAL RESULTS

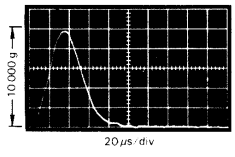

TYPICAL SYSTEM:

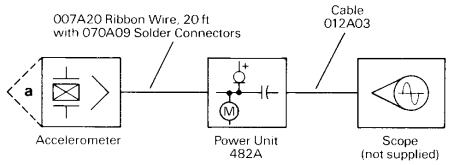

PCB PIEZOTRONICS, INC. 3425 WALDEN AVENUE DEPEW, NEW YORK 14043-2495 TELEPHONE 716-684-0001 TWX. 710-263-1371

FIGURE A-1: Specifications for the high-shock accelerometer that was used as a triggering mechanism on the sledge hammer seismic source.

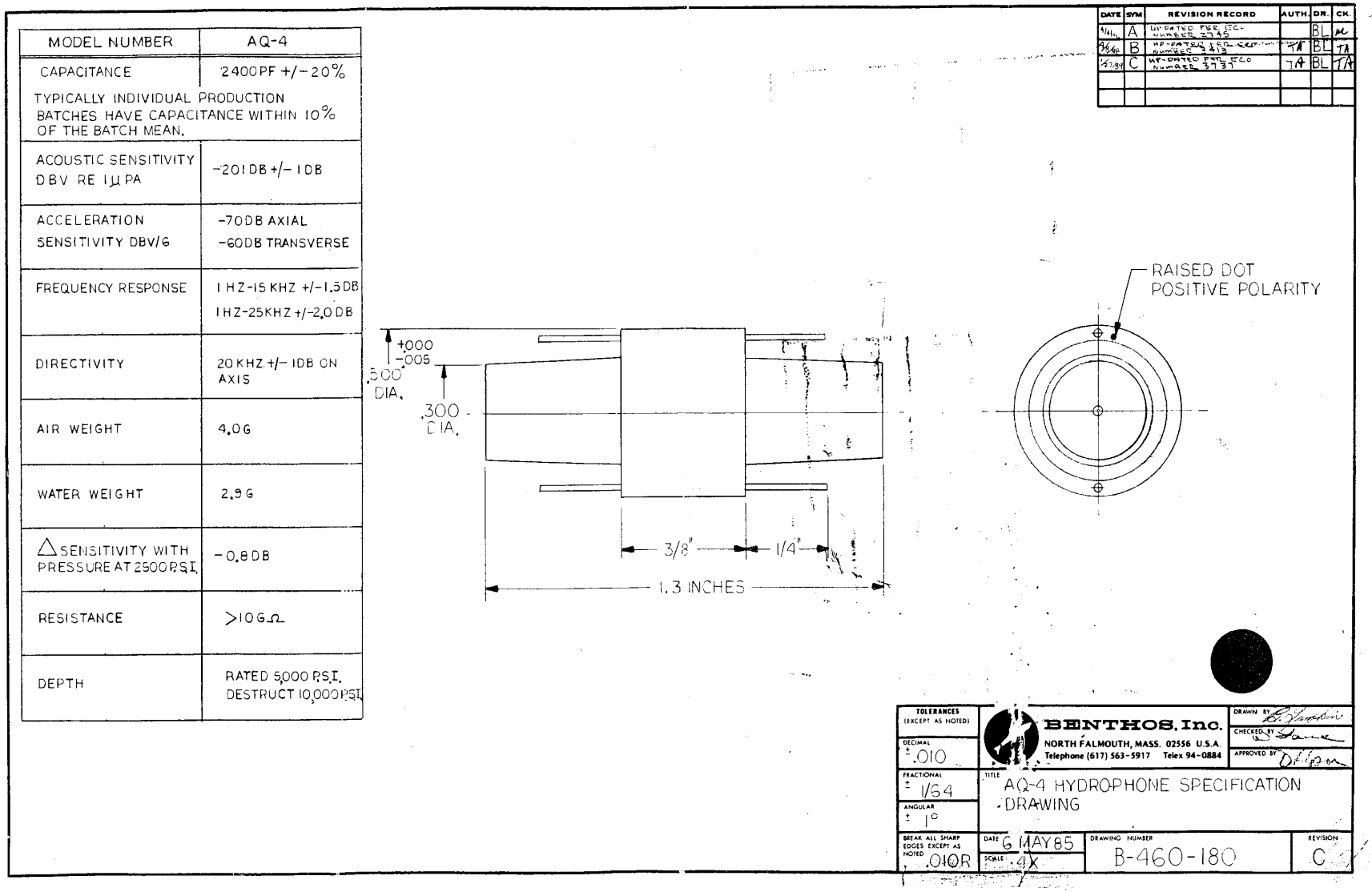

FIGURE A-2: Specifications for the piezoelectric transducers used inside the hydrophone string.

Matrix-5 Technologies, Inc.
12687 West Cedar Drive, Suite 220
Lakewood, CO 80228
(303) 987-2713

USBR CUSTOM HYDROPHONE AMPLIFIER SPECIFICATIONS

These model HYDAMP-C amplifiers are designed to accept the signal from a hydrophone sensor cartridge using very short twisted-pair leads and to produce a high-level differential analog signal on the output pair. Special EMI shielding fabric was incorporated to form a skirt around the sensor cartridge to significantly reduce 60-Hertz mains noise pickup. These units accept an unregulated bipolar DC supply and are reverse-polarity protected. The entire circuit-board is potted for rough-handling and installation in oil-filled downhole flexible tubing for normal submersible use.

Summary of specifications:

Equivalent input noise of pre-amplifier stage: 3 nV / Hz^0.5
Equivalent input impedance: 40 megohms
Equivalent DC gain: 32 dB (26 dB plus 6 dB for differential line-driver)
Cable drive capability: 2000 feet of 30 pF/ft (supply-rails at +8 and -8 VDC)
Hydrophone sensor equivalent capacitance matching: 2200 pF
Bandwidth: 200 KHz
Low-frequency cutoff: 1000 Hz
Power-supply: +11-18 VDC and -11-18 VDC unregulated
Potting material: Epoxy Technology Inc., 'Epo-Tek 509'

FIGURE A-3: Specifications for the hydrophone amplifiers.

Model Number	QUARTZ SHEAR ICP® ACCELEROMETER SPECIFICATIONS	Revision: H
353B17		ECN #: 7752

DYNAMIC PERFORMANCE			
Voltage Sensitivity	mV/g [mV/(m/s²)]	10 [1,02]	(±10%)
Measurement Range	±g pk [±m/s² pk]	500 [4 905]	
Frequency Range: (±5%)	Hz	1 to 10,000	
(±10%)	Hz	0.7 to 20,000	
(±3 dB)	Hz	0.35 to 30,000	
Mounted Resonant Frequency	kHz	≥70	
Resolution - Broadband	g pk [m/s² pk]	0.01 [0,1]	
Amplitude Linearity	%	±1	[1]
Transverse Sensitivity	%	≤5	[2]
ENVIRONMENTAL			
Shock Limit (Maximum)	±g pk [±m/s² pk]	10,000 [98 100]	
Operating Temperature Range	°F [°C]	-65 to +250 [-54 to +121]	
Temperature Response		See Graph	[3]
Strain Sensitivity	g/με [(m/s²)/με]	≤0.002 [≤0,02]	
ELECTRICAL			
Excitation Voltage/Constant Current	VDC/mA	18-30/2-20	
Output Impedance	ohms	<100	
Output Bias	VDC	8 to 12	
Discharge Time Constant	sec	≥0.5	
Warm Up Time (within 10% of output bias)	sec	<5	
Broadband Electrical Noise: (1-10 kHz)	μV rms	40	
Spectral Noise: (1 Hz)	μg/√Hz [(μm/s²)/√Hz]	3,200 [31 392]	[4]
(10 Hz)	μg/√Hz [(μm/s²)/√Hz]	700 [6 867]	
(100 Hz)	μg/√Hz [(μm/s²)/√Hz]	180 [1 766]	
(1 kHz)	μg/√Hz [(μm/s²)/√Hz]	64 [628]	
Ground Isolation	ohms	None (Optional)	
MECHANICAL			
Sensing Element	material/geometry	Quartz/Shear	
Housing	material/sealing	Titanium/Welded	
Size (hex x height)	inch [mm]	0.28 x 0.55 [7,1 x 14,0]	
Weight	oz [gm]	0.06 [1,7]	
Electrical Connector	type/location	2-Pin Solder/Top	
Cable (standard 10 ft supplied)	type/termination	031D010W Twisted Pair/10-32	
Mounting Thread	size	5-40 Male	
Mounting Torque	**in-lb [N-cm]**	**8-12 [90-135] Must Be Applied**	

PCB® PIEZOTRONICS

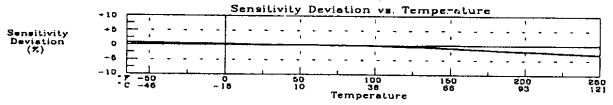

In the interest of constant product improvement, we reserve the right to change specifications without notice.

℗ is a registered trademark of PCB Piezotronics, Inc.

OPTIONAL VERSIONS

Optional versions have identical specifications and accessories as listed for the standard model except where noted by the letter prefixes below. More than one option may be used.

☐ **A - Adhesive Mount**
Additional Accessory: (1) Model 080A90 "quick bonding gel"
Note: Adhesive mounting base is not required.

☐ **B - Low Output Bias**

Output Bias	VDC	4.5 - 6.5	
Excitation Voltage/Constant Current	VDC/mA	12 - 30/1 - 20	
Measurement Range	±g pk [±m/s² pk]	300 [2 943]	
Resolution-Broadband	g pk [m/s² pk]	0.02 [0,2]	
Broadband Electrical Noise: (1-10 kHz)	μV rms	120	
Spectral Noise: (1 Hz)	μg/√Hz [(μm/s²)/√Hz]	4,600 [45 126]	[4]
(10 Hz)	μg/√Hz [(μm/s²)/√Hz]	1,120 [10 987]	
(100 Hz)	μg/√Hz [(μm/s²)/√Hz]	460 [4 513]	
(1 kHz)	μg/√Hz [(μm/s²)/√Hz]	130 [1 275]	

☐ **J - Ground Isolated**

High Frequency Range: (+5%)/(+10%)	Hz	8,000/15,000
Mounted Resonant Frequency	kHz	≥56
Electrical Base Isolation	ohms	>10⁸
Size (hex x height):	inch [mm]	0.37 x 0.69 [9,5 x 17,5]
Weight	oz [gm]	0.10 [2,9]

☐ **M - Metric**
Mounting Thread: size: M3 x 0.5 Male
Supplied Accessories: (1) Model M080A15 base replaces Model 080A15

☐ **Q - Extended Time Constant**

Low Frequency Range: (-5%)/(-10%)	Hz	0.15/0.1
Discharge Time Constant:	sec	≥5
Warm Up Time (within 10% of output bias)	sec	45

☐ **W - Water Resistant**
Cable (standard 10 ft supplied): type/termination: 018D010A/10-32

NOTES:
[1] Zero based best straight line method.
[2] Transverse sensitivity is typically ≤3%.
[3] Specification within ±2% of typical curve.
[4] Acceleration level equivalent.

SUPPLIED ACCESSORIES:
080A15 Adhesive Mounting Base (1)
(except A option)
080A24 Petro Wax Sample (1)
NIST Traceable Calibration Certificate

Drawn:	Engineer:	Sales: CSA	Approved:	Spec Number:
Date: 4/3/97	Date: 03APR97	Date: 4/3/97	Date: 4/3/97	353-2170-80

FIGURE A-4: Specifications for the receiver accelerometers.

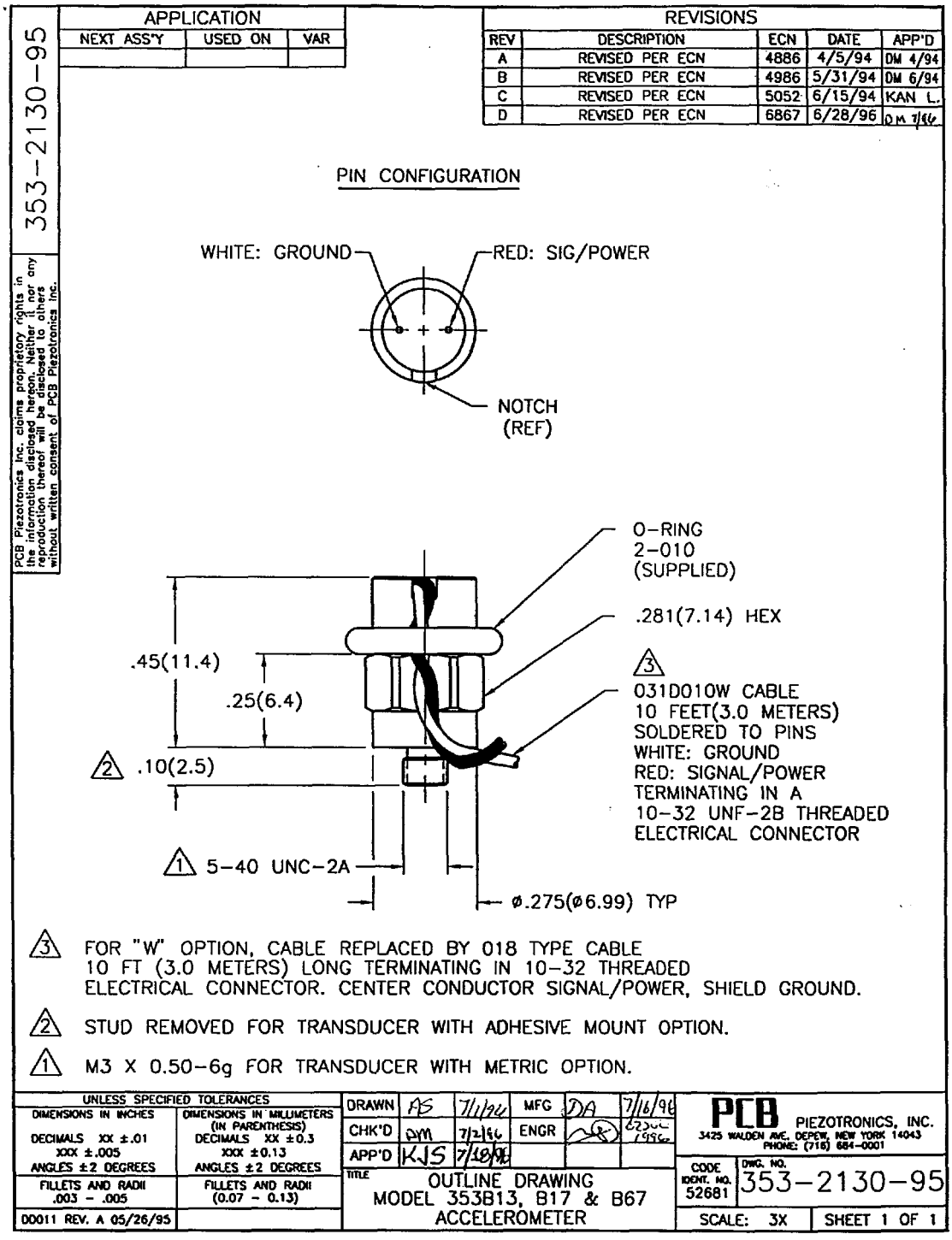

FIGURE A-4, continued.

Matrix-5 Technologies, Inc.
12687 West Cedar Drive, Suite 220
Lakewood, CO 80228
(303) 987-2713

USBR CUSTOM ACCELEROMETER AMPLIFIER SPECIFICATIONS

These model ACCAMP-C amplifiers are designed to accept the signal from PCB three-wire accelerometers and to produce a high-level differential analog signal on the output pair. A current-source power-supply for the accelerometer is integral. These units accept an unregulated bipolar DC supply and are reverse-polarity protected. The entire amplifier is provided as a printed-circuit-board with card-edge connectors at each end for ease of service/replacement. Provision is made for external gain-setting resistors.

Summary of specifications:

Equivalent input noise of pre-amplifier stage: 3 nV / Hz^0.5
Equivalent max DC gain: 33 dB (27 dB plus 6 dB for differential line driver)
(Gain = 1 + R2/R1, R2 = Rext parallel 2.2K, R1 = 100)
Cable drive capability: 2000 feet of 30 pF/ft (supply-rails at +8 and -8 VDC)
Bandwidth: 200 KHz
Low-frequency cutoff: 500 Hz
Power-supply: +11-18 VDC and -11-18 VDC unregulated

FIGURE A-5: Specifications for the accelerometer amplifiers.

Matrix-5 Technologies, Inc.
12687 West Cedar Drive, Suite 220
Lakewood, CO 80228
(303) 987-2713

SPECIFICATIONS FOR HSDAS-16-20 DATA-ACQUISITION SYSTEM

This system consists of 20 channels capable of concurrent sampling at up to 80,000 16-bit samples/second (12.5 uS per sample). The memory depth is 450Kb or 225K samples -- 2.8 seconds at the maximum rate. In effect, the total memory available is 10 Mbytes. Each channel consists of a dedicated low-power microcomputer and a low-noise, programmable-gain optically-isolated analog-to-digital card. Each micro-computer is equivalent to an IBM XT running 10 times faster than the original XT (the TERN Inc. model AE-40). All the channels are controlled by and uploaded to an industrial PC which employs a parallel bus connection to all channels for high-speed parallel data-transfer.

The internal rails are +15 and -15 volts so the input buffers can accept +/- 10 volt signals. The gain is programmable (from a user menu) from 0 dB to 48 dB in 6 dB steps.

Both the input control-signals and output parallel data-signals are optically-isolated with high-speed HP opto-couplers. In this way the analog circuits do not share any common or ground with any digital circuits; even the power-supply is specially designed to maintain full isolation.

Some control-functions are implemented on a high-speed serial bus running at 115Kb; i.e., sample-rate and pre-trigger time and the like are parameters sent to the microcomputers using a simple command-protocol.

The analog and digital connections are implemented with both D-sub connectors and circular-metal-shell 'military' connectors. The D-sub connectors allow easy testing and re-configuring of channels; i.e., re-mapping sources to different acquisition channels.

The industrial PC runs a graphical user interface in a DOS environment. This approach reduced development time and cost and allowed easier revision of the various C-language programs, batchfiles, and user-menus. Drivers, written in assembly language, were developed for the high-speed parallel bus, the high-speed serial bus, and to meet the specialized triggering requirements. Triggering can be done using an external window-comparator trigger-detector device capable of fast rising-edge (either polarity) detection.

FIGURE A-6: Specifications for the seismic data acquisition system.

APPENDIX B

PHOTOGRAPHS TAKEN DURING THE SEISMIC TOMOGRAPHY SURVEYS AT SEMINOE DAM, WYOMING

FIGURE B-1: View of the upstream side of Seminoe Dam (August 2000).

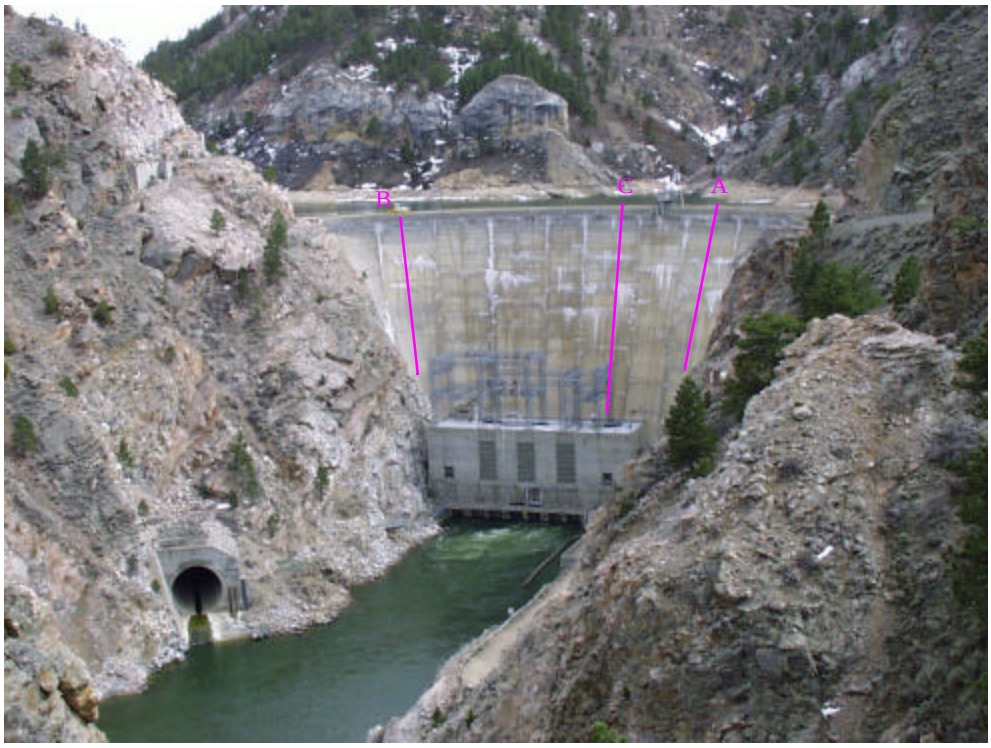

FIGURE B-2: Downstream face of Seminoe Dam, with the approximate locations of the seismic tomography cross sections overlaid (April 1999).

FIGURE B-3: Installation of the accelerometers on the upstream face (April 1999).

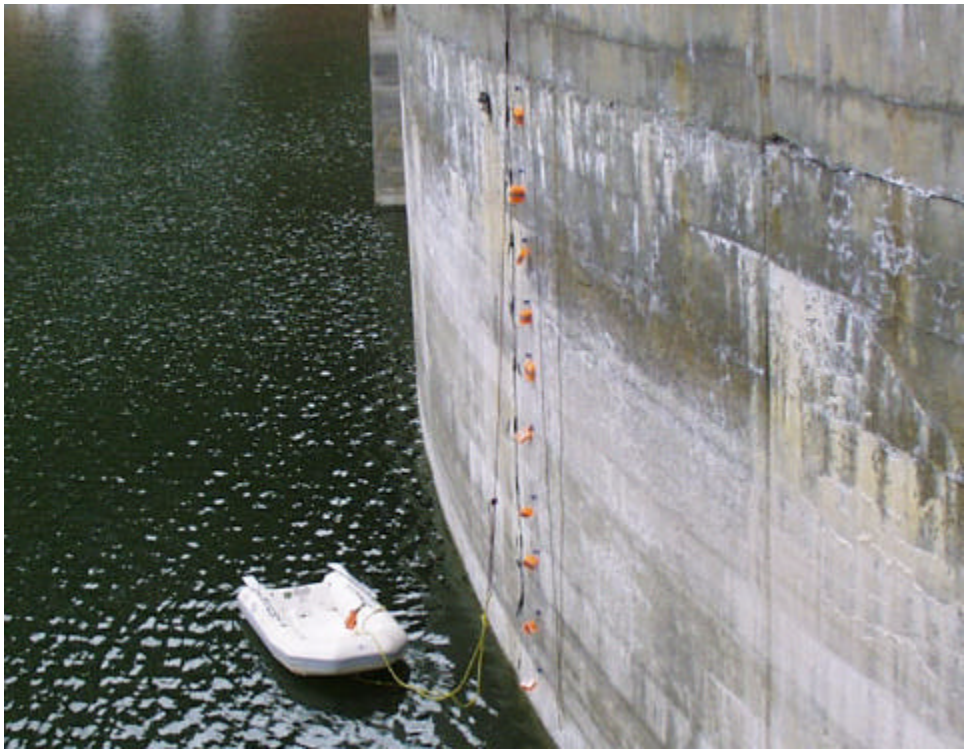

FIGURE B-4: Accelerometers mounted on the upstream face (April 1999).

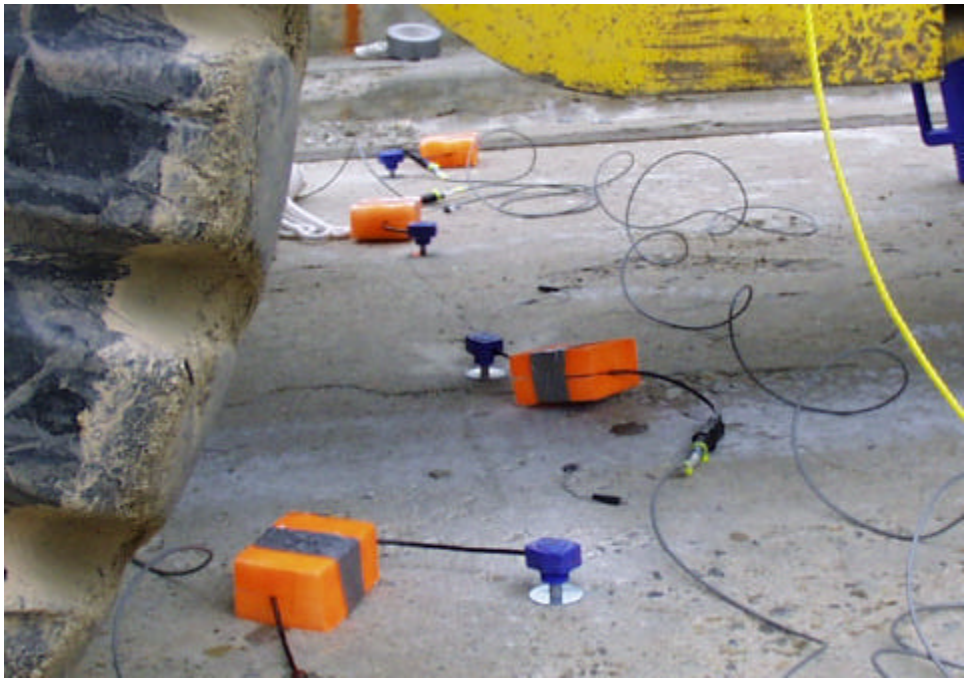

FIGURE B-5: Accelerometers mounted across the crest (April 1999).

FIGURE B-6: Hydrophone string (April 1999).

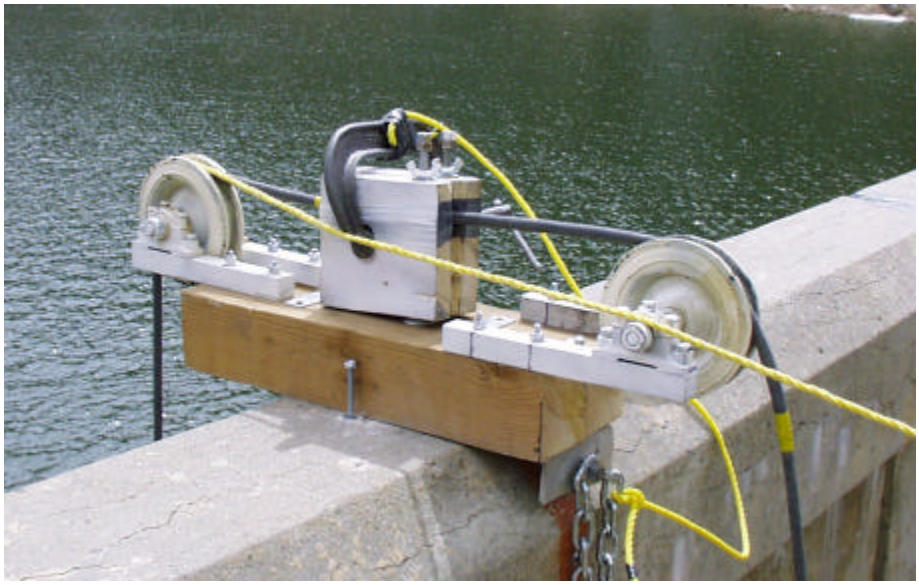

FIGURE B-7: Device for passing the hydrophone cable over the parapet wall and clamping the cable to maintain a specified hydrophone depth (April 1999).

FIGURE B-8: Using the nail gun seismic source on the downstream face (April 1999).

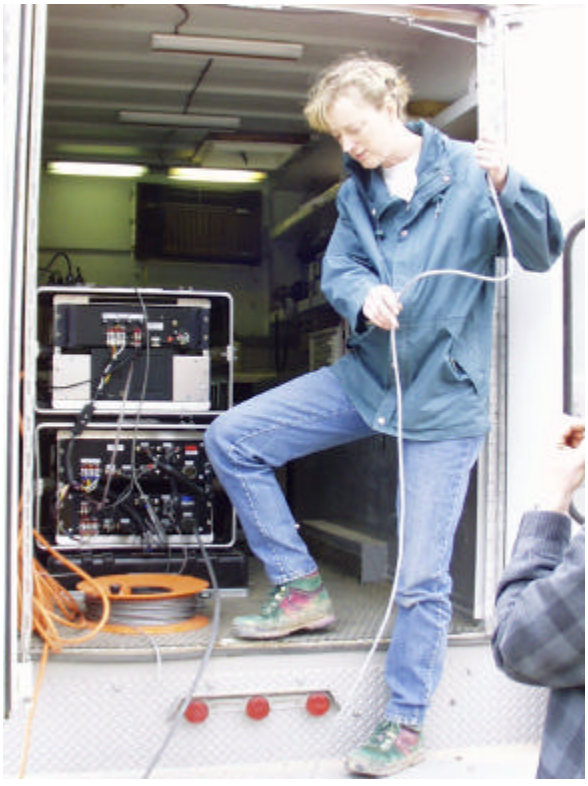

FIGURE B-9: Seismic data acquisition system in the back of the truck (April 1999).

FIGURE B-10: 1000-lb weight lowered to the bottom of the reservoir to anchor the hydrophone positioning line (August 2000).

APPENDIX C

MATHEMATICAL FORMULATION OF THE ARRIVAL-TIME SEISMIC RAY TOMOGRAPHY METHOD

Forward Problem

In ray-based seismic tomography, the infinite-frequency limit is used to model seismic wave propagation. In this model, the seismic energy is assumed to propagate along ray paths that can be represented by discrete lines. The P-wave ray paths are computed using the source and receiver locations and a specified P-wave velocity structure. The velocity structure for a seismic tomography cross section is represented by a two-dimensional (2-D) grid of constant-velocity pixels. The velocities are assumed to project unchanged outside the tomography plane (a 2 1/2 - D model). Although the velocities vary only in two dimensions, three-dimensional ray tracing is performed in cases where the source or receiver locations are offset from the tomography plane. The ray tracing method of Saito (1989), based on determining the path of minimum travel time, was modified for three dimensions and is used to compute ray paths and travel times.

Inverse Problem

Because seismic waves propagate along paths that are strongly influenced by the velocity structure, seismic arrival-time tomography is a nonlinear inverse problem. The nonlinear inversion is performed by iteratively solving the constrained, linearized problem. Let t_{obs}= an observed arrival time, t_{calc} = the corresponding calculated arrival time based on the current velocity model, and r = the residual = t_{obs} - t_{calc}. The goal is to change the velocities so that the change in calculated arrival time, $\Delta t_{calc,}$ is equal to the residual, r. Expanding Δt_{calc} in terms of changes in the velocities and keeping only the first-order terms gives:

$$\sum_{j=1}^{npixels} \frac{\partial t}{\partial v_j} \Delta v_j = \sum_{j=1}^{npixels} \frac{-l_j}{v_j^2} \Delta v_j = r, \qquad (1)$$

where v_j is the P-wave velocity of the jth pixel and l_j is the length of the ray segment in the jth pixel. Both sides of equation (1) are divided by $\sqrt{|r|}$ to obtain an approximate L1-norm optimization (Scales et al., 1988). The equation is also weighted according to the quality of the arrival time pick, which is determined from the signal-to-noise ratio of the seismic waveform. In addition, a residual cut-off is employed to discard extreme outliers. The arrival times for all seismic traces yield a set of equations that can be put into matrix form:

$$\boldsymbol{M}\overline{Dm} = \bar{h}. \qquad (2)$$

The matrix $\boldsymbol{M}$ contains the weighted partial derivatives, the vector h contains the weighted residuals, and the solution vector $\overline{\Delta m}$ contains the velocity perturbations.

To prevent extreme fluctuations of the velocities of poorly resolved pixels, velocity regularization is included in the inversion. This regularization is a weighted constraint that requires the velocity model to have a controlled degree of smoothness. The regularization is implemented by minimizing the first-order spatial velocity derivatives. Similar methods have been used by others (Lees, 1989; Sambridge, 1990; Phillips and Fehler, 1991). The numerical velocity derivative for one consecutive pair of velocity pixels is given by:

$$[(v_i + \Delta v_i) - (v_{i-1} + \Delta v_{i-1})] / d, \qquad (3)$$

where v_i and v_{i-1} are the velocities of 2 consecutive velocity pixels in one coordinate direction, and d is the distance between the centers of the pixels. Equations for all consecutive pixels in

each coordinate direction are constructed. The velocity derivatives may be expressed as a matrix equation involving the solution vector $\overline{\Delta m}$:

$$\textit{spatial velocity derivatives} \;=\; \bar{c} + \boldsymbol{K}\overline{\Delta m}. \qquad (4)$$

The vector *c* contains the numerical velocity derivatives based on the current model, and the matrix **K** contains numerical derivative operators.

The constrained L1-norm solution is found by minimizing

$$\sum(\textit{weighted arrival time residuals})^2 + \lambda\sum(\textit{spatial velocity derivatives})^2,$$

which is expressed mathematically by

$$(\boldsymbol{M}^T\boldsymbol{M} + \lambda\boldsymbol{K}^T\boldsymbol{K})\overline{\Delta m} \;=\; (\boldsymbol{M}^T\bar{h} - \lambda\boldsymbol{K}^T\bar{c}). \qquad (5)$$

Equation 5 is solved using a general conjugate gradient algorithm. The velocities are updated using the velocity perturbations given by $\overline{\Delta m}$, and the procedure is repeated until the arrival time residuals no longer improve significantly.

The parameter λ is a weighting factor that determines the degree of smoothness of the final velocity model. A large value of λ results in a smooth velocity model, but the arrival times may not be well-satisfied (i.e., the arrival time residuals may be large). Multiple seismic tomography inversions are performed using progressively smaller values of λ. The velocity model determined from one inversion is used as the starting model for the next inversion. The inversions are stopped when the arrival time residuals are approximately equal to the estimated uncertainty in the observed arrival times, or the velocity model becomes unreasonably variable.

References

Lees, J. M. Seismic tomography in western Washington, *Ph. D. Thesis*, University of Washington, 1989.

Phillips, W. S., and M. C. Fehler. Traveltime tomography: A comparison of popular methods, *Geophysics*, vol. 56, 1991, 1639-1649.

Saito, H. Traveltimes and raypaths of first-arrival seismic waves: Computation method based on Huygen's principle, in *59th Ann. Internat. Mtg., Soc. Expl. Geophys., Expanded Abstracts*, 1989, 244-247.

Sambridge, M. S. Nonlinear arrival-time inversion: Constraining velocity anomalies by seeking smooth models in 3-D, *Geophys. J. Int.*, vol. 102, 1990, 653-677.

Scales, J. A., A. Gersztenkorn, and S. Treitel. Fast l_p solution of large, sparse, linear systems: Application to seismic traveltime tomography, *J. Comp. Phys.*, vol. 75, 1988, 314-333.